Upgrading recovered carbon black (rCB) from industrial-scale end-of-life tires (ELTs) pyrolysis to activated carbons: Material characterization and

Citation for the original published paper (version of record):
Dziejarski, B., Hernández-Barreto, D., Moreno-Piraján, J. et al (2024). Upgrading recovered carbon black (rCB) from industrial-scale end-of-life tires (ELTs) pyrolysis to activated carbons: Material characterization and CO<inf>2</inf> capture abilities. Environmental Research, 247. http://dx.doi.org/10.1016/j.envres.2024.118169

Environmental Research 247 (2024) 118169

Contents lists available at ScienceDirect

Environmental Research

journal homepage: www.elsevier.com/locate/envres

Upgrading recovered carbon black (rCB) from industrial-scale end-of-life tires (ELTs) pyrolysis to activated carbons: Material characterization and CO_2 capture abilities

Bartosz Dziejarski[a,b,c,*], Diego Felipe Hernández-Barreto[d], Juan Carlos Moreno-Piraján[d,*], Liliana Giraldo[e], Jarosław Serafin[f], Pavleta Knutsson[c], Klas Andersson[b,g], Renata Krzyżyńska[a]

[a] *Faculty of Environmental Engineering, Wroclaw University of Science and Technology, 50-370, Wroclaw, Poland*
[b] *Department of Space, Earth and Environment, Division of Energy Technology, Chalmers University of Technology, SE-412 96, Gothenburg, Sweden*
[c] *Department of Chemistry and Chemical Engineering, Division of Energy and Materials, Chalmers University of Technology, SE-412 96, Gothenburg, Sweden*
[d] *Departamento de Química, Facultad de Ciencias, Grupo de Investigación en Sólidos Porosos y Calorimetría, Universidad de Los Andes, Cra. 1a No. 18A-10, Bogotá D.C. 11711, Colombia*
[e] *Departamento de Química, Grupo de Calorimetría, Universidad Nacional de Colombia, Sede Bogotá, Cra. 45, Bogotá D.C. 11711, Colombia*
[f] *Department of Inorganic and Organic Chemistry, University of Barcelona, Martí I Franquès, 1-11, 08028, Barcelona, Spain*
[g] *Department of Chemical Engineering, University of Utah, Salt Lake City, UT, USA*

ARTICLE INFO

Keywords:
Tire recycling
Circular economy
Sustainable materials
Waste management
CO_2 adsorption
Net-zero emissions

ABSTRACT

The current study presents for the first time how recovered carbon black (rCB) obtained directly from the industrial-scale end-of-life tires (ELTs) pyrolysis sector is applied as a precursor for activated carbons (ACs) with application in CO_2 capture. The rCB shows better physical characteristics, including density and carbon structure, as well as chemical properties, such as a consistent composition and low impurity concentration, in comparison to the pyrolytic char. Potassium hydroxide and air in combination with heat treatment (500–900 °C) were applied as agents for the conventional chemical and physical activation of the material. The ACs were tested for their potential to capture CO_2. Ultimate and proximate analysis, Fourier-transform infrared spectroscopy (FT-IR), scanning electron microscopy with energy dispersive X-ray spectroscopy (SEM-EDS), Raman spectroscopy, thermogravimetric analysis (TGA), and N_2/CO_2 gas adsorption/desorption isotherms were used as material characterization methods. Analysis revealed that KOH-activated carbon at 900 °C (AC-900K) exhibited the highest surface area and a pore volume that increased 6 and 3 times compared to pristine rCB. Moreover, the AC-900K possessed a well-developed dual porosity, corresponding to the 22% and 78% of micropore and mesopore volume, respectively. At 0 °C and 25 °C, AC-900K also showed a CO_2 adsorption capacity equal to 30.90 cm^3/g and 20.53 cm^3/g at 1 bar, along with stable cyclic regeneration after 10 cycles. The high dependence of CO_2 uptake on the micropore volume at width below 0.7–0.8 nm was identified. The selectivity towards CO_2 in relation to N_2 reached high values of 350.91 (CO_2/N_2 binary mixture) and 59.70 (15% CO_2/85% N_2).

1. Introduction

Waste treatment of end-of-life tires (ELTs) flows constitute a crucial challenge due to the rapid development of the automotive and transportation sectors and limited infrastructure for disposal and recycling (Dabic-Miletic et al., 2021; Martínez, 2021; Trudsø et al., 2022). ELTs contribute roughly 2% of the total waste generated around the globe (Karaağaç et al., 2017), with 1.6 billion tires being manufactured and discarded in a single year 2020 and the market demand that continues to rise (Global Tire Recycling Market Analysis, 2020). It is suggested that 75% of ELT waste is deposited in landfills without being subjected to any treatment (Ferdous et al., 2021), which can potentially lead to fire

---

* Corresponding author at: Faculty of Environmental Engineering, Wrocław University of Science and Technology, 50-370 Wrocław, Poland; Department of Space, Earth and Environment, Division of Energy Technology, Chalmers University of Technology, SE-412 96 Gothenburg, Sweden.

* Corresponding author at: Departamento de Química, Facultad de Ciencias, Grupo de Investigación en Sólidos Porosos y Calorimetría, Universidad de Los Andes, Cra. 1a No. 18A-10, Bogotá D.C. 11711, Colombia

E-mail addresses: bartoszd@chalmers.se (B. Dziejarski), jumoreno@uniandes.edu.co (J.C. Moreno-Piraján).

https://doi.org/10.1016/j.envres.2024.118169
Received 10 November 2023; Received in revised form 14 December 2023; Accepted 9 January 2024

hazards, breeding grounds for mosquitoes and other pests, and/or release chemicals that have a negative impact on air, ground, and water (Bulei et al., 2018; Mohajerani et al., 2020). Rubber, which constitutes a significant proportion of tires (approximately 60–65%) (Tian et al., 2021), represents a highly stable material with degradation process in soil that may require 800–2000 years (Basik et al., 2021). Among existing waste treatment methods (reuse of whole tires, feedstock recycling, and energy recovery), pyrolysis has shown to be a promising alternative for waste treatment (Hoang et al., 2022). This process represents the thermal decomposition of organic substances at temperature of 400 °C–650 °C without oxidizing agent (Premchand et al., 2023), which allows the recovery of valuable substances. These substances include gases (H_2, H_2S, or C1–C4 light hydrocarbons), condensable oil, as well as carbonaceous solid residues (Singh et al., 2018; Kandasamy et al., 2015). In the case of ELTs pyrolysis, the solid phase (pyrolytic char) represents a share of about 35% of the overall good (Yang et al., 2022). The obtained pyrolytic char needs to be further refined to gain recovered carbon black (rCB) with the high value of elemental carbon. The main driver behind the growth of the interest in rCB is the escalating demand for sustainable substitutes to virgin carbon black (vCB) which is ranked among the top 50 commercial chemicals on a global scale (Cardona-Uribe et al., 2021). The production of rCB acquired from ELTs renders thus a more environmentally viable option than vCB, which is sourced from fossil fuels and characterized with high CO_2 footprint as well as results pollutant emissions (SO_x, NO_x and PM). Hence, the application of sustainable rCB has successfully transitioned into industrial implementation, playing a significant role in achieving circularity within the tire sector.

One of the possible reuses of recovered black carbon is as activated carbons (ACs). Activated carbons are a unique type of carbon-based materials with a wide range of applications, such as for water purification (Jjagwe et al., 2021), energy storage (Ayinla et al., 2019), and separation of flue gas mixtures (Mukherjee et al., 2019). Additionally, ACs exhibit a wide array of desirable properties, including an extensive network of pores, well-developed microporosity, a high surface area, and significant chemical or thermal characteristics, which can find applications in multiple fields. Activated carbons have also been proposed as a cost-effective and efficient alternative to conventional sorbents, such as amine-based solvents for carbon dioxide capture (Kishibayev et al., 2021; Serafin et al., 2017, 2021, 2023a; Abuelnoor et al., 2021). ACs can be synthesized through two well-known processes: physical and chemical activation (Dziejarski et al., 2023). Physical activation frequently involves carbon dioxide, water vapor, air, or combinations thereof. Air is commonly reported as a favorable activation agent due to its availability, low cost, and eco-friendliness. It is typically used at lower temperatures, ranging from 450 °C to 700 °C (Plaza et al., 2014; Ould-Idriss et al., 2011; Gomez-Serrano et al., 1993; Zabaniotou et al., 2008), depending on the precursor and the desired properties of the resulting AC. On the other hand, chemical activation agents that are most often cover KOH, K_2CO_3, H_3PO_4, and $ZnCl_2$. Potassium hydroxide is considered as the most effective in terms of the development of porosity and surface area, where the optimal temperature range is generally higher and typically between 750 °C and 900 °C (Serafin et al., 2022a; Sangchoom and Mokaya, 2015; Shen et al., 2018; Ogungbenro et al., 2020).

Commonly, ACs are produced from biomass residue, because it is considered an abundant and renewable precursor material. However, biomass waste flows are heterogeneous and have a composition that differs significantly depending on the geographical region. On average, the carbon content in biomass is approximately 45–50% by weight, which may be considered fairly low. Biomass-based ACs are usually developed with the aim of fabricating perspective goods that extend beyond the mitigating of environmental degradation, such as addressing the issue of ELTs disposal. Previous studies have addressed the valorization of discarded waste tires in laboratory conditions. These investigations have also explored the turning of the resulting pyrolytic char into activated carbons. Sun et al. (1997) used scrap tires treated with by both physical and chemical activation methods, such as the use of CO_2 and KOH. The materials were then applied for the storage of natural gas. Teng, Lin, and Hsu (Teng et al., 2000) focused on ACs synthesized by KOH impregnated as a means of exploring the correlation between the devolatilization conditions and their porous structure. Moreover, several other researchers made contributions to this field, including Stavropoulos (2005), Hofman and Pietrzak (2011), López et al. (2013), and Nieto-Márquez et al. (2016). Their works have mostly concentrated on examining the adsorption capacities of the waste tires based ACs for a range of chemicals, such as, e.g., methylene blue, cyclohexane, and major air pollutants (sulphur dioxide, or nitrogen dioxide). Although the outcomes present ACs derived from ELTs pyrolysis as a potentially effective solution for waste management, there is a gap in the literature on the direct conversion of tailor-made rCB transformed from contaminated soot on industrial sector. This gap extends to possible ways for its application when it comes to CO_2 capture, as the most significant greenhouse gas. Research conducted in this specific field has the opportunity to demonstrate rCB/AC production as an industrial ready, economically viable process, and explore their potential utilization for CO_2 capture, which is also the aim of this paper.

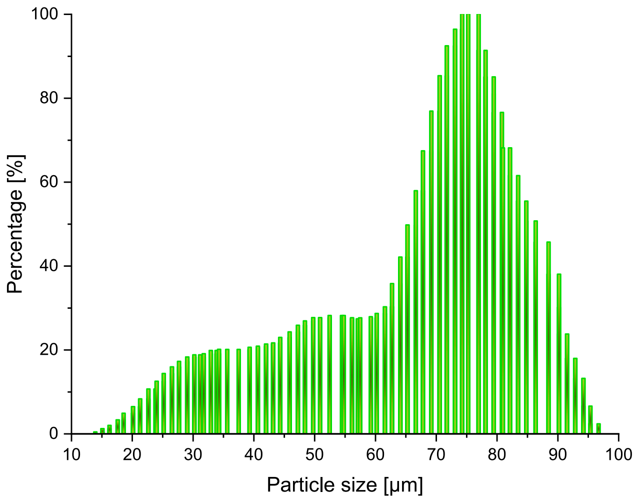

Fig. 1. Histogram of particle size distribution for recovered carbon black.

The current work shows for the first time rCB conversion from industrial-scale ELTs pyrolysis to ACs for the application of CO_2 emission reduction. By upgrading the rCB to ACs, this approach addresses the ecological concerns related to ELTs at the same time as it makes use of a valuable resource available on the commercial market. Thus, the strategy presented is particularly important in the context of circular economy and resource conservation. The upgraded rCB/ACs are expected to exceed the low boundaries for activated carbons quality derived from waste tire char or various types of biochars. This is closely related to having a standardized original composition, which can result in a repetitive production of high-quality material with improved characteristics, such as a high fixed carbon content and lower impurity and ash levels. As a consequence, while conventional ACs have well-established CO_2 adsorption capabilities, rCB/ACs can exhibit comparable or even higher performance. Additionally, the use of rCB/ACs presents an opportunity to adopt a resource-efficient and responsible method for managing the waste streams generated from the treatment of ELTs. This is particularly advantageous because of the easily accessible rCB. Finally, the results presented in this study contribute to the development of solid adsorbents by simultaneously transforming one of the most widely available global waste into a value-added product. These value-added rCB/ACs can be further improved and potentially applied for CO_2 capture.

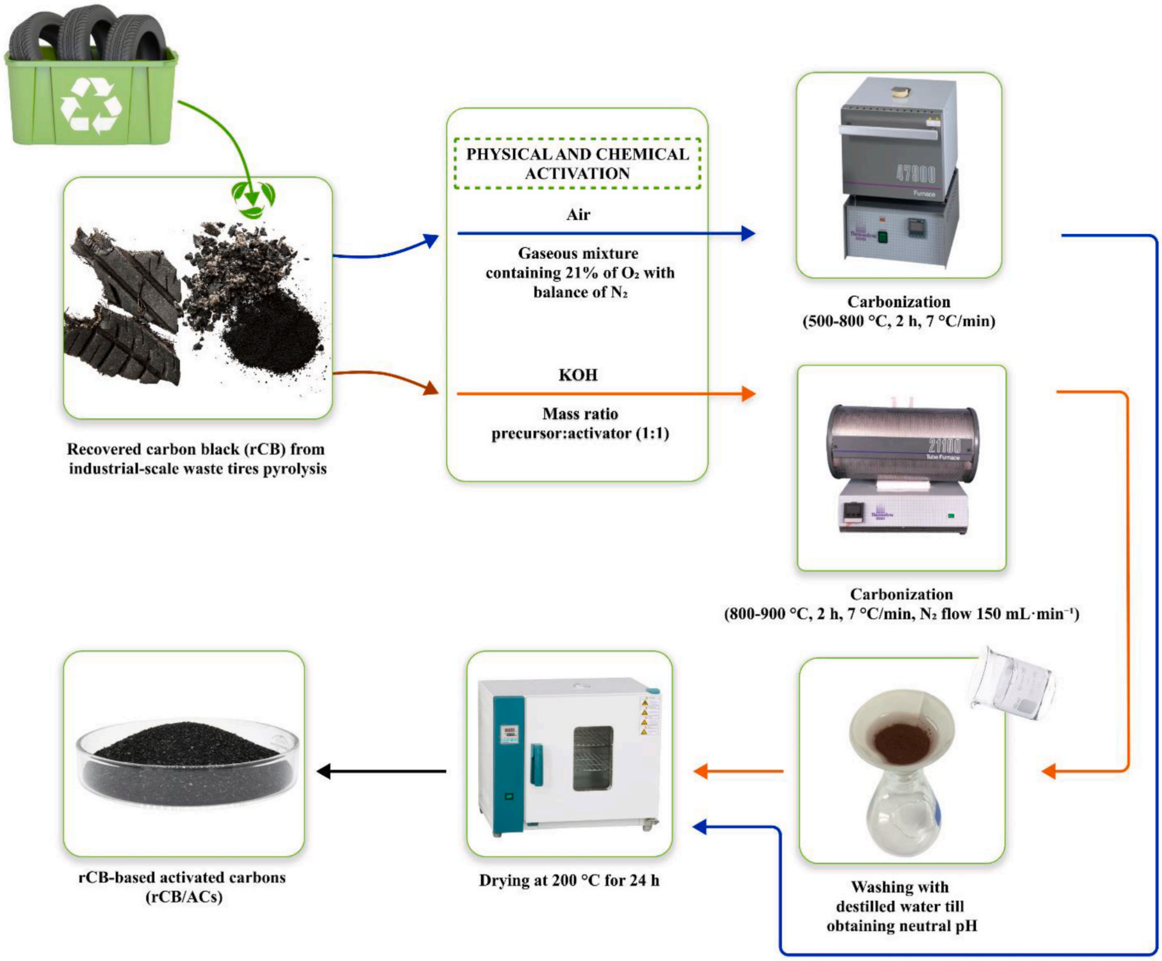

Fig. 2. Schematic representation of the preparation procedures used for activation of rCB/ACs based on recovered carbon black (rCB).

2. Materials and experiment methodology

2.1. Raw material

The recovered carbon black with an average particle size of 30 μm and an ash content equal to 0.5–2% was used as the activated carbon precursor, supplied by Syntoil company located in Poland. To fabricate it, a treatment of char (devolatilization, milling, and optional pelleting) was applied to remove the ash content, metal contaminants, and standardize the particle size variability. As can be observed in Fig. 1, rCB consists mainly of particle sizes of 73–80 μm in the range of 15–100 μm that are the most abundant in its volume. Chemical composition of rCB is variable, depending on composition of tires utilized in pyrolysis, where the main component is carbon in a variety of 92–99.5%. Besides it may also consist of volatile substances with a content of $>$0.2%, and mineral matter of approximately 0.5–2%, including, among others, silicon, aluminium, zinc, sulphur and calcium.

2.2. Preparation of rCB/AC samples

Activated carbons were prepared from rCB without any additional pre-preparations by physical and chemical activation via air and KOH, as shown in Fig. 2. For physical activation, a Barnstead Thermolyne 47900 muffle was used, and the effect of the activation temperature was studied. The temperature was changed from 500 to 700 °C in atmospheric air (gaseous mixture containing 21% of O_2 with balance of N_2), with a heating rate of 7 °C·min^{-1} and a dwelling time of 2 h. In the case of chemical activation, potassium hydroxide (KOH) was used as the activating agent through a dry mixing method. Equivalent mass quantities of rCB and KOH (mass ratio 1:1) were grounded on a mortar to obtain a homogeneous solid mixture. The 1:1 ratio served as a crucial reference point to establish a baseline and initial assessment of KOH activation behavior stages for the rCB material. The activation was then performed using a Barnstead Thermolyne 21100 tubular horizontal furnace, under an inert atmosphere (N_2) and with a constant flow of 150 mL min^{-1}. The temperatures were set at 800, 850 and 900 °C, holding for 2 h with a heating rate of 7 °C·min^{-1}. The chemically activated carbons obtained were washed several times with deionized water until a constant pH of the washing water was obtained. Finally, all obtained rCB/ACs were dried in oven for 24 h at 200 °C. rCB/ACs samples were labelled AC-XXXZ, where XXX is the activation temperature, and Z corresponds to the activating agent (potassium hydroxide (K) or air (A)).

2.3. Characterization of carbon materials

2.3.1. Textural characterization

In order to analyze the textural properties of the synthesized AC samples, N_2 physisorption isotherms at −196 °C were measured using a Micromeritics ASAP 2020 Plus Adsorption Analyzer. Samples were degassed previous the analysis by two heating steps: the first one (evacuation phase) was carried out at a maximum temperature of 110 °C, under vacuum (10^{-8} bar) and for 1 h. After that the second step (heating phase) reached a temperature of 300 °C for 9h and under vacuum. Then the isotherms were acquired measuring around 40 adsorption points and 20 desorption points from a relative pressure (P/P_0) of $1{\cdot}10^{-6}$. The specific surface area was calculated using the

Table 1
Description of selected adsorption isotherm models.

Isotherm model	Described adsorption phenomenon	Non-linear model equations	Characterization of equation	Ref.
Freundlich-Langmuir	Considering both monolayer and multilayer adsorption effects	$q_e = \frac{q_m \bullet K_{FL} \bullet P^{n_{FL}}}{1 + K_{FL} \bullet P^{n_{FL}}}$	q_m - maximum adsorption capacity (cm^3/g), K_{FL} - Langmuir-Freundlich constant (bar $^{-nFL}$), n_{FL} - index of heterogeneity [-]	Nuhnen and Janiak (2020)
Redlich–Peterson	Includes the features of both Langmuir and Freundlich isotherm	$q_e = \frac{K_{RP} \bullet P}{1 + a_{RP} \cdot P^{\beta_{RP}}}$	K_{RP} - Redlich-Peterson constant ($cm^3 \cdot g^{-1} \cdot bar^{-1}$), a_{RP} - constant (bar $^{-\beta RP}$) β_{RP} - Redlich–Peterson exponent (–)	Cai et al. (2022)
Toth	Multi-layered sorption on heterogeneous surfaces at both low and high pressure.	$q_e = \frac{q_m \bullet K_T \bullet P}{[1 + (K_T \bullet P)^{n_T}]^{\frac{1}{n_T}}}$	K_T - Toth constant (bar^{-1}), n_T – heterogeneity factor (–)	Aniruddha et al. (2020)
Sips	Combined form of the Langmuir and Freundlich model equations to characterize heterogeneous adsorption systems	$q_e = \frac{q_m \bullet (K_S \bullet P)^{\frac{1}{n_S}}}{1 + (K_S \bullet P)^{\frac{1}{n_S}}}$	K_S - Sips constant (bar^{-1}), n_S – Sips exponent (–)	Mukherjee and Samanta (2019)
Radke–Prausnitz	Adsorption with low concentration of the gas molecules	$q_e = \frac{q_m \bullet K_{RPr} \bullet P}{(1 + K_{RPr} \cdot P)^{e_{RPr}}}$	K_{RPr} - Radke–Prausnitz constant (bar^{-1}), e_{RPr} - Radke–Prausnitz exponent (–)	Khoshraftar and Ghaemi (2023)

Brunauer - Emmett - Teller (B.E.T) equation in the range of relative pressure of 0.05–0.3. The NLDFT model was used to determine the pore size distribution (PSD) and the micropore and mesopore specific volumes. Micropore analysis was complemented by measuring CO_2 adsorption isotherms at 0 °C.

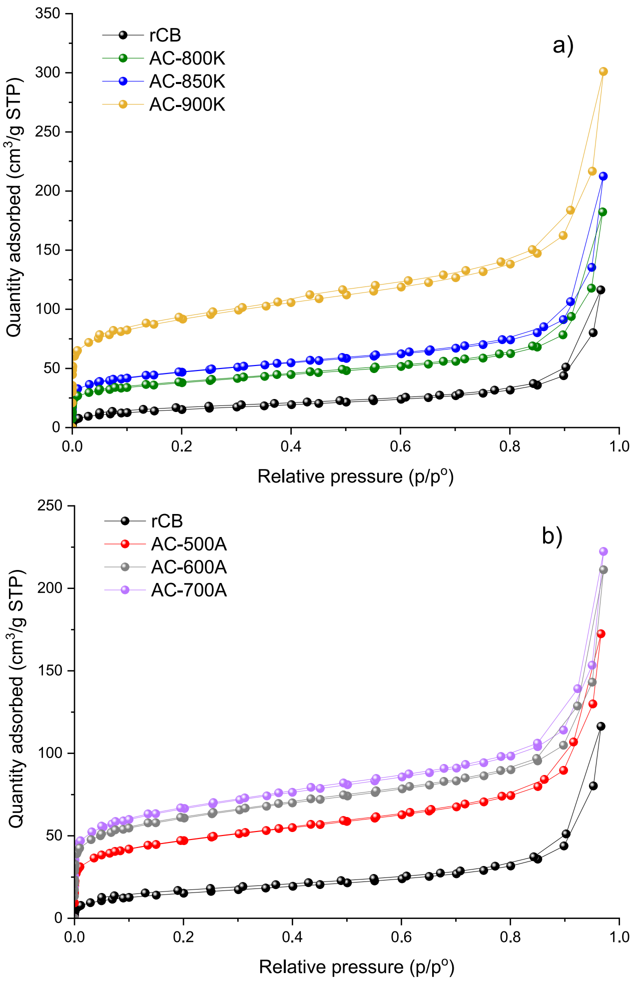

Fig. 3. N_2 adsorption-desorption isotherm curves at −196 °C of the prepared activated carbons samples by (a) chemical activation, (b) physical activation.

2.3.2. *Chemical characterization*

The ultimate analyses were done using a CHNS Elemental Analyzer FLASH 2000 from Thermo Fisher Scientific. To conduct an analysis of potassium amount, the X-ray fluorescence energy dispersion spectrophotometer (EDXRF) of the Epsilon 3 model, manufactured by PANalytical B, was used. Moreover, the proximate analysis was performed with TGA.

To investigate the interactions and functional groups present on ACs that are relevant to the CO_2 adsorption, Fourier-transform infrared spectroscopy (FT-IR) was applied. FT-IR was performed using a Shimadzu IRTracer-100 spectrometer equipped with the Diffuse Reflectance Accessory, DiffusIR™. The spectra were acquired with 100 scans, a resolution of 1.93 cm^{-1} between 400 and 4000 cm^{-1}, and under nitrogen to avoid absorption of water during the analysis. Carbon-based materials were crushed and mixed with KBr to obtain solid dissolutions with a concentration of 1 % w/w, and each dissolution was analyzed in the spectrometer.

For evaluation of the decomposition and thermal stability of AC materials used for CO_2 capture application, thermogravimetric analysis (TGA) was also utilized. TGA was studied using the thermal analyzer TGA 550 from TA Instruments, with a nitrogen flow of 150 mL min^{-1}, a heating rate of 10 °C·min^{-1} and a temperature range of 20–900 °C.

2.3.3. *Morphological characterization*

Surface morphologies and differences in the shapes of the activated carbon surfaces were observed through the Scanning-Electron Microscopy (SEM). SEM images were acquired using a TESCAN LYRA3 FIB-SEM microscope coupled to a microanalysis system of Energy-Dispersive X-ray spectroscopy (EDS) and using both, backscattering electrons, and secondary electrons detectors. Samples were previously metal-coated to improve electrical conductivity. To evaluate the structure of the carbon skeleton in the obtained carbon materials, Raman spectroscopy measurements were performed. The measurements were done using a Horiba Xplora Raman microscope via a laser with a wavelength of 523 nm, 100x of magnification, and 70% of the laser power to avoid sample's damage.

2.4. *CO_2 adsorption investigation*

CO_2 adsorption isotherms were measured using the Micromeritics ASAP 2020 Plus Sorption Analyzer. Analysis temperature was set to 0, 15, 25 and 30 °C using a water bath contained on a Dewar flask. Absolute pressure was changed from 5×10^{-4} to 1 bar and samples were degassed previous the analysis with the same conditions as before, which are 110 °C under vacuum (10^{-8} bar) and for 1 h prior to analysis.

Table 2
Textural parameters of the rCB-based activated carbons.

Sample	BET surface area[a], m^2/g	Total pore volume[b], cm^3/g	Micropore volume [c] $_{(<2\ nm)}$, cm^3/g	Supermicropore volume [d] $_{(0.7–2nm)}$, cm^3/g	Ultramicropore volume [d] $_{(<0.7\ nm)}$, cm^3/g	Micropore volume$_{(<2\ nm)}$/total pore volume, %	Mesopore volume/ total pore volume, %
rCB	55	0.170	–	–	–	–	–
AC-800K	131	0.275	0.036	0.021	0.015	13	87
AC-850K	165	0.316	0.048	0.028	0.020	15	85
AC-900K	328	0.448	0.100	0.069	0.031	22	78
AC-500A	161	0.253	0.050	0.029	0.021	20	80
AC-600A	218	0.327	0.066	0.042	0.024	20	80
AC-700A	232	0.333	0.072	0.047	0.025	22	78

[a] Brunauer, Emmett & Teller (BET) method using the Rouquerol criteria.
[b] Calculated by N_2 adsorption isotherm at a high relative pressure (~0.99).
[c] DFT method via NLDFT model, assuming slit-shaped pores, based on N_2 adsorption isotherm at −196 °C.
[d] DFT method via NLDFT model, assuming slit-shaped pores, based on CO_2 adsorption isotherm at 0 °C.

Furthermore, the ideal adsorption solution theory (IAST) was employed to determine the CO_2/N_2 adsorption selectivity of the ACs (vital aspect for CO_2 capture application) based on N_2 sorption measurement at a temperature of 25 °C.

2.5. CO_2 adsorption mechanism studies

To identify CO_2 adsorption mechanism, experimental results were fitting the Toth, Freundlich-Langmuir, Sips, Redlich-Peterson, and Radke-Prausnitz isotherm models, using a nonlinear regression method by the quasi-newton algorithm incorporated in the Matlab ® function, fmincon. Table 1 provides a comprehensive presentation of the non-linear form of isotherm equations, along with their theoretical assumptions and parameter description. The adequacy of the chosen theoretical model in relation to the empirical data was assessed by the sum of absolute errors (EABS) that is common modeling tool of adsorption isotherms. The EABS is presented by the below formula:

$$EABS = \sum_{i=1}^{n} \left| q_{e,\exp} - q_{e,mod} \right| \tag{1}$$

Where: qe,$_{mod}$ - predicted amount of adsorbed adsorbate at equilibrium state [cm^3/g], qe,$_{exp}$ - experimental amount of adsorbed adsorbate at equilibrium state [cm^3/g].

Furthermore, the thermodynamic parameters of adsorption were calculated using the van't Hoff equation and Clausius-Clapeyron equations for CO_2 adsorption isotherms at 0, 15, 25 and 30 °C, which are the most widely reported estimation approach for Gibbs free energy, enthalpy, entropy, and isosteric heat of adsorption.

3. Results and discussion

3.1. Studies of textural properties by N_2 adsorption/desorption isotherms at −196 °C and CO_2 adsorption at 0 °C

The textural characteristics of prepared rCB/ACs was examined using N_2 adsorption and desorption measurements at a temperature of −196 °C. Fig. 3 (a,b) schematically illustrates the N_2 isotherms for all samples produced in the temperature range of 800–900 °C and 500–700 °C by applying chemical and physical activation, respectively. Through the examination of isotherms, the crucial adsorption characteristics of materials can be evaluated, simultaneously enabling the design and optimization of adsorbents to effectively adsorb CO_2. Hence, to evaluate the required textural properties for effective CO_2 adsorption, presented methodology focuses on two key factors: the necessity of sufficient surface area with porosity, and the specific range of pore sizes. It is widely reported that materials with high surface areas and tailored pore structures, especially microporosity with pore width below 0.7 nm, are highly beneficial and desirable for CO_2 adsorption (Boujibar et al., 2019; Plaza et al., 2010). The N_2 isotherm data was analyzed to determine the extent of porosity development within the material, assessing the efficiency for CO_2 capture. By examining the shape, steepness, and hysteresis of the isotherms, the valuable insights were gain into the porosity evolution.

The materials were characterized by a rapid increase in adsorption at low relative pressures ($P/P_0 < 0.1$), which is followed by a gradual growth along with P/P_0 values and the appearance of a loop. The shapes of the N_2 sorption isotherm curves correspond to the combination of type I and IV (Baldovino-Medrano et al., 2023; Muttakin et al., 2018). Type I suggests the development of activated carbon with micropore content (<2 nm in diameter) in which a primary filling occurs at very low relative pressure values, as confirmed by a very steep isotherm with a sharp knee below $P/Po < 0.15$ (Ozpinar et al., 2022). Type IV is a variant of type II but has a discrete multilayer structure that corresponds to mesoporous materials (with pores of 2–50 nm) and gives a characteristic hysteresis loop (Soltani et al., 2019). Consequently, upon achieving a P/Po value of 1.0, indicating a further gradual reduction in pressure, a discernible desorption curve is formed, which is distinguishable from the one that results from the initial adsorption. This phenomenon is highly associated to filling empty mesopores by capillary condensation (Dantas et al., 2019).

Moreover, as can be seen, all isotherms exhibit H3-type hysteresis in an almost complete range of P/P_0 above 0.35, which is especially visible between 0.8 and 1.0 region. These findings strongly indicate that the pore size distributions are nearly analogous to those of combination of micro- and mesopores, including aggregates of plate-like particles forming to slit-shaped pores with non-uniform size and shape (Yousif et al., 2022). Hence, the outcome implies the existence of a dual porosity of the ACs produced from rCB, revealing that the carbon structure is characterized by both well-developed micropores and mesopores.

The textural properties of rCB/ACs are summarized in Table 2. The results of the textural characteristics of activated carbons relative to rCB, as the raw material, confirmed the optimal enhancement of the BET surface area by 83% and the total pore volume by 64%, accordingly. Additionally, all ACs primarily presented a percentage of mesoporosity, ranging from 78 to 87% of the porous structure. As observed, raising the activation temperature led to an increase in BET surface area, total pore volume, and microporosity, which was reported in many other studies (Serafin et al., 2023b; Wang et al., 2020). The augmentation of the

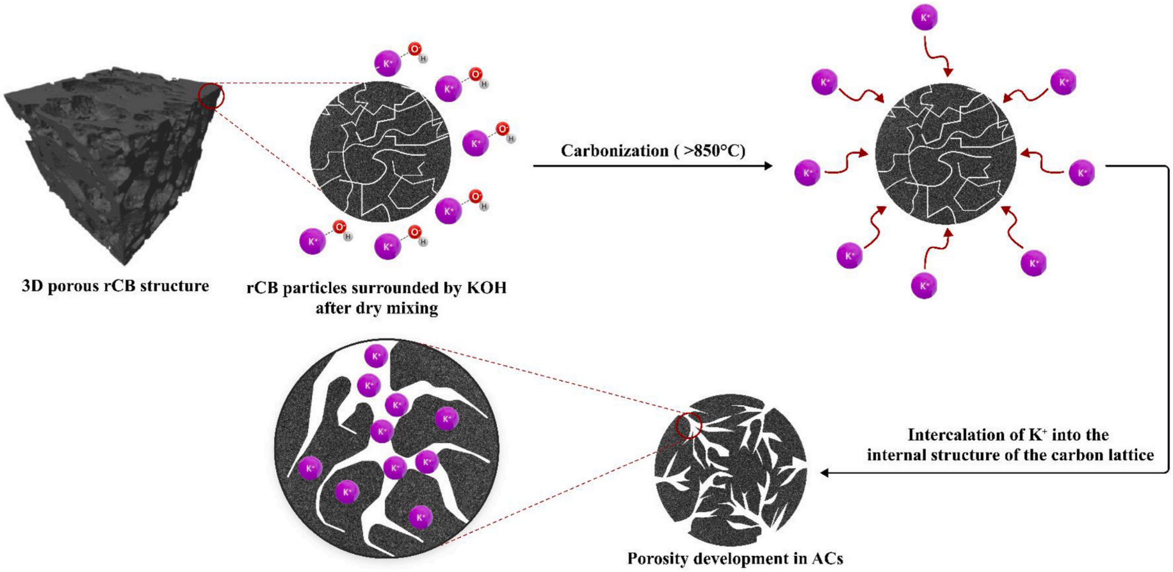

Fig. 4. Schematic Illustration of pore formation mechanism in rCB during chemical activation using KOH.

activation temperature caused a boost in the reactivity of the carbon atoms situated on the surface of the rCB. This, in turn, led to an acceleration of the diffusion rate of activating agent molecules transportation inside the material (Lan et al., 2019).

In the case of physical activation, AC-700A was found to be the best sample due to its the greatest textural parameters, followed by AC-600A and AC-500A. On the other hand, among chemically activated samples with KOH, AC-900K synthesized at 900 °C demonstrated the highest Brunauer-Emmett-Teller surface area, total pore and micropore volume (pores up to 2 nm determined by N_2 adsorption at −196 °C) of 328 m^2/g,

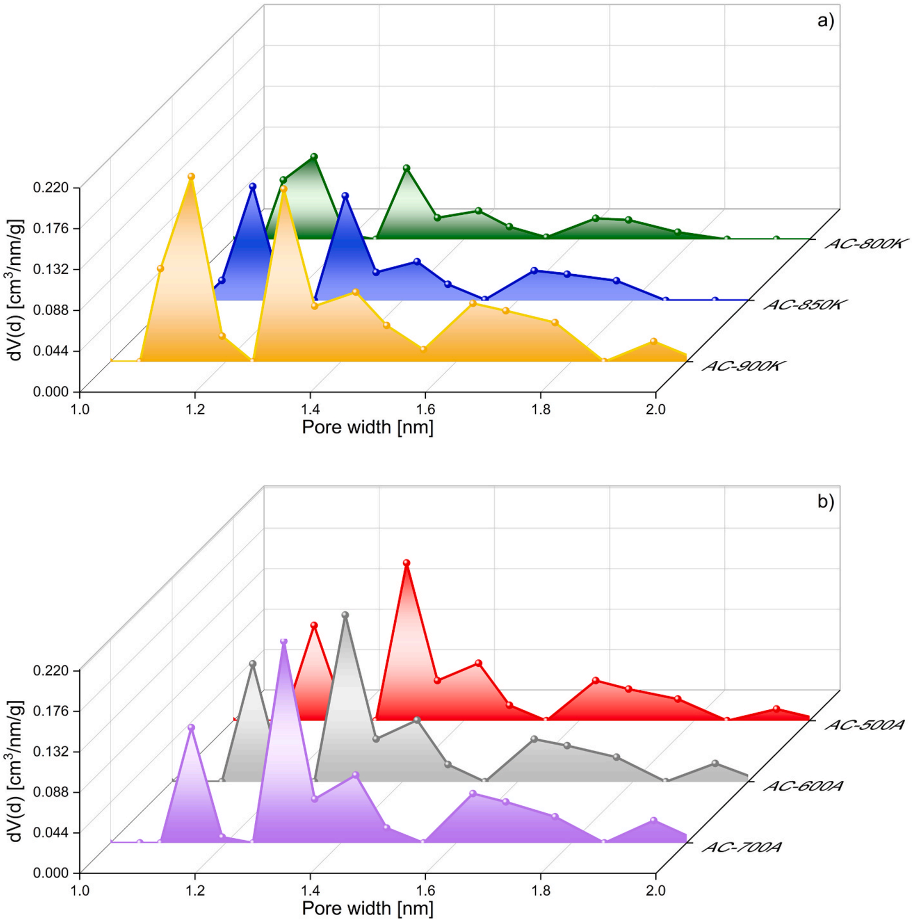

Fig. 5. Pore size distribution within a width of 1–2 nm for activated carbons obtained by (a) chemical activation, (b) physical activation, determined with the NLDFT method based on N_2 sorption at − 196 °C.

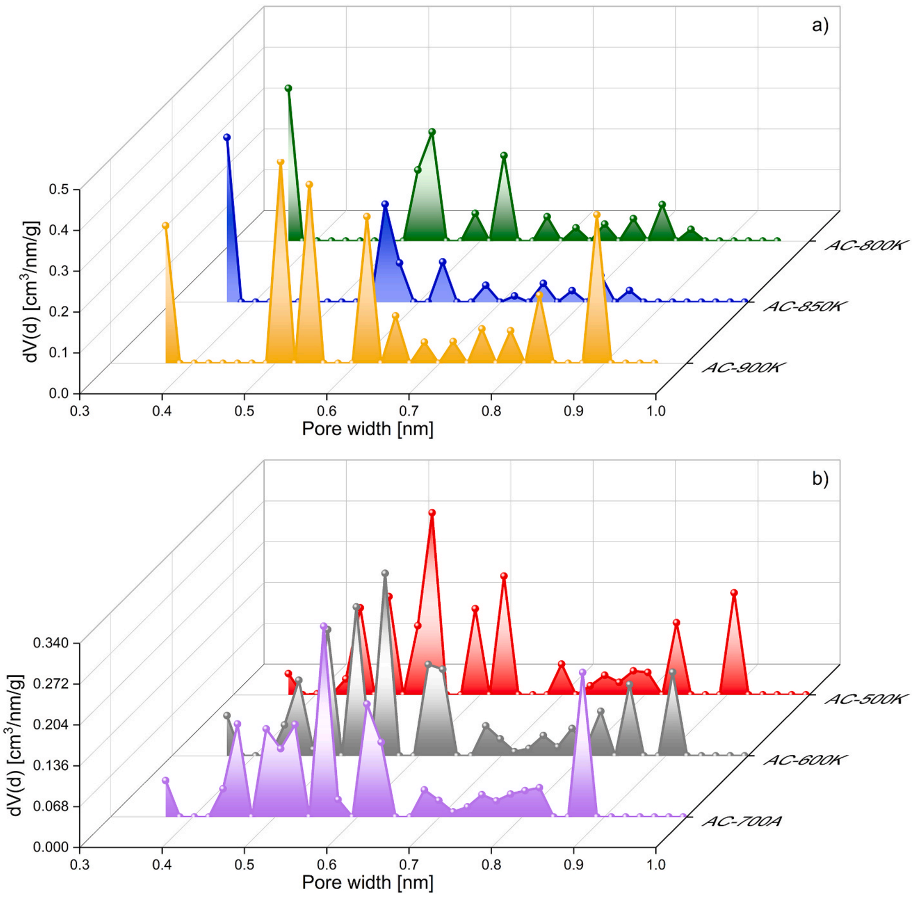

Fig. 6. Pore size distribution within a width below 1 nm for activated carbons obtained by (a) chemical activation, (b) physical activation, determined with the DFT method based on CO_2 sorption at 0 °C.

0.448 cm^3/g, and 0.100 cm^3/g, respectively.

The quite noticeable development of the specific surface area and porosity between 700 and 900 °C according to the literature may be closely related to the formation of metallic potassium (>762 °C) (Arslanoğlu, 2019), which is a significant factor in the generation of the pore framework (Mistar et al., 2020). Exceeding the temperature from 850 to 900 °C improved the micropore content to 22%. This can happen when vapor of metallic K is assimilated and diffused into the internal structure of the carbon particles and predominantly graphitic layers, which eventually leads to the manifestation of new porosities and the stretching of the pores that already exist (Fig. 4). With the generally accepted mechanism, during activation most of KOH is transformed into K_2CO_3 and K_2O, as follows (Gao et al., 2020):

$$2KOH \rightarrow K_2O + H_2O \tag{2}$$

$$K_2O + CO_2 + C \rightarrow K_2CO_3 \tag{3}$$

$$4KOH + C \rightarrow K_2CO_3 + K_2O + 2H_2 \tag{4}$$

Then by their reduction by carbon atoms, potassium is obtained, according to the below equations (Li et al., 2017):

$$K_2O + C \rightarrow 2K + CO \tag{5}$$

$$K_2CO_3 + C \rightarrow 2K + 3CO \tag{6}$$

On the other hand, at 800–900 °C and KOH/AC ratio of 1:1, KOH-ACs should exhibit much higher surface area and micropore volume compared carbons prepared by using air. This suggests that specific ratio between rCB and KOH along with the temperature may need to be further optimized to achieve the right balance between activation and preservation of the desired rCB/ACs porosity characteristics.

3.2. Pore size distribution (PSD) analysis

Further, in order to determine the pore size distributions (PSD) of all AC samples, a non-local density functional theory (NLDFT) model assuming slit pores was also employed. The PSDs obtained from N_2 adsorption measurements at −196 °C are plotted in Fig. 5 and Figure S1 for a pore width range below 2 nm and within 2–35 nm. In line with the graphs, the majority of the pores are nearly completely varied across the spread distribution that is comparatively placed within entire range of 35 nm. The PSD curves indicate that a significant proportion of pores are classified as mesopores in total, while there is a smaller number of micropores, which are relatively large in the combined structure of ACs. The micropore widths are primarily concentrated within the range of 1.05–1.19, and 1.25–1.54 nm, as proven by the two most prominent peaks at 1.14 and 1.30 nm. On the contrary, the mesopore diameters are predominantly situated within the 2.30–3.90, 9.48–10.36, 12.36–13.50 nm, and evidently focused between 16.00 and 34.05 nm spectrum.

PSD determination has conventionally been performed through nitrogen sorption isotherms obtained at −196 °C, as above. However, the diffusion rate of nitrogen molecules into micropores of small size is significantly reduced at low temperatures, and the estimation of pores with width below 1 nm is not feasible. The aforementioned issue can be resolved by performing CO_2 adsorption at a temperature of 0 °C. At elevated temperatures and increased absolute pressures, the accessibility of ultramicropores by CO_2 molecules exceeds that of N_2 at −196 °C, despite the similarity in molecular critical dimensions between the two gases. Therefore, this method provides insight into the characteristics of pores that fall within the diameter range of approximately

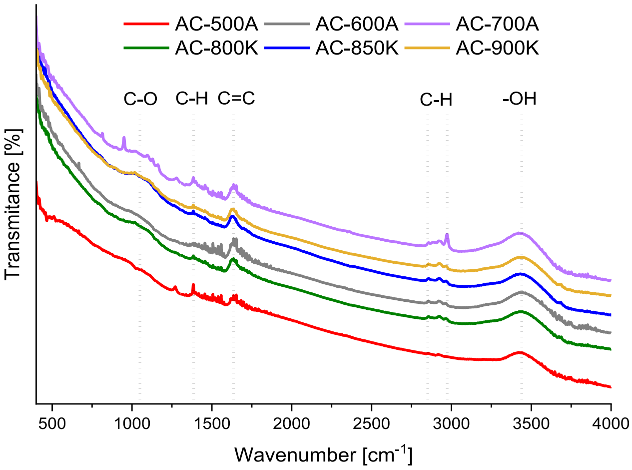

Fig. 7. FT-IR spectra of rCB/AC materials.

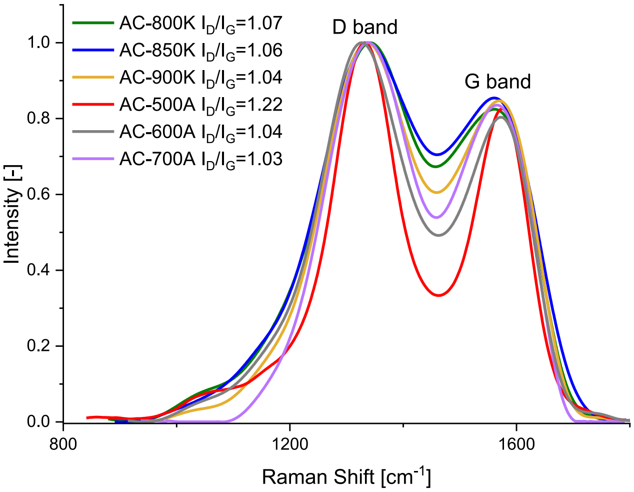

Fig. 8. Raman spectra of rCB/AC materials.

0.3–1 nm. Fig. 6 show PSDs based on CO_2 adsorption at 0 °C determined by using also the DFT method. All rCB/ACs obtained via chemical activation are distinguished by the presence of two distinct peaks that exhibit high intensity at pore diameters measuring approximately from 0.37 to 0.38 nm, and 0.49–0.59 nm. Additionally, AC-900K and AC-850K also exhibited higher pore volume within 0.87–0.91 and 0.61–0.64 nm. For physical activated AC samples, the predominant pore size in the AC-700A was determined to be between 0.44 and 0.64 nm, with a few single distinct peaks above 0.83 nm. The results of the study reveal that the use of potassium hydroxide and air during the activation process is particularly conducive to the formation of supermicropores (0.7–2 nm) and ultramicropores (<0.7 nm), indicating a high content level. In the AC-900K and AC-700A, pores with widths ranging from 0.7 to 2 nm accounted for the majority at 69% and 66% of the microporosity, while pores less than 0.7 nm wide constituted 31% and 34%, respectively. Conversely, they exhibit a relatively lower suitability for the creation of submicropores (<0.4 nm), which manifest a limited number of distinct peaks, however, quite high for the AC-900K.

3.3. *Fourier-transform infrared spectroscopy (FT-IR)*

Using Fourier transform infrared spectroscopy (FT-IR), the surface functional groups of rCB/ACs were analyzed. Fig. 7 illustrates the FT-IR spectra between 450 and 4000 cm^{-1}, revealing the diverse surface chemistry of the ACs. The FT-IR spectroscopy analysis indicate that the AC samples exhibit similar characteristic absorption peaks, with predominant vibrations observed in the range of 3550-3350 (O–H), 3000-2850 (C–H), 1700-1600 (C=C), 1400-1350 (C–H), 1100-1000 (C–O) cm^{-1}.

The occurrence of a broad band at 3450 cm^{-1} corresponds to the presence of an O–H stretching vibration in free hydroxyl groups on the carbon surface, which can be attributed to the effect of chemical and physical activation (Kajal and Singh, 2019). This vibration is commonly observed as a direct influence of intermolecular hydrogen bonding of chemical compounds, including alcohols, phenols, and carboxylic acids (Gonzalez et al., 2009). Furthermore, the two strong bands observed at within 3000-2850 and at 1380 cm^{-1} are related to the bending vibrations of the C–H bonds of alkanes groups (Talik et al., 2020), simultaneously providing information about the AC structure. Similarly, the band at 1650 cm^{-1} represents C=C stretching vibrations from aromatic rings frequently found in carbonaceous materials (Sricharoenchaikul et al., 2008). The infrared spectra of the ACs also present the occurrence of C–O stretching vibration appearing near the really broad peak region between 1100 and 1000 cm^{-1} (Xuguang, 2005).

The determined absorption bands in all samples were found to be located at comparable wavenumbers, suggesting a high degree of similarity in the functional groups. FTIR spectra indicated the presence of oxygen-containing surface functional groups (OCFG) that are extremely useful for CO_2 adsorption application purposes in flue gas purification. Taking into consideration the fact that OCFG are the most prevalent groups on carbon surfaces, the C–O and O–H bonds should be given a significant amount of focus. Especially, hydroxyl groups can enhance the interaction between CO_2 and the carbon surface through hydrogen bonding and are typically associated with increased CO_2 adsorption capacity (Yue et al., 2008). In overall, the surface reactivity and acidity/basicity of AC can be tremendously influenced by the presence of OCFG, thereby affecting its adsorption towards different gaseous adsorbates.

3.4. *Raman spectroscopy*

Raman spectroscopy is applied for the insights into the crystal structure of carbon-based materials, such as the degree of graphitization, or the presence of defects. Fig. 8 illustrates the Raman spectra of all activated carbon samples. The Raman spectra investigation of rCB/ACs revealed the existence of two distinct bands, located at approximately 1330 cm^{-1} (D-band) and 1590 cm^{-1} (G-band) wave numbers. These peaks in carbonized structures are referred to as the disordered (D) band and graphitic (G) band, according to the literature that has been widely published (Wang et al., 1990; Bhattacharjya et al., 2014). The D-band is commonly correlated with breaking of symmetry in sp^2 carbon caused by the structural defects and disorders in the carbon framework, leading to a reduction in the crystallographic symmetry of the quasi-infinite lattice (Brown et al., 2001). The precise nature of the vibrational mode responsible for the D-band arise from a breathing mode of the A_{1g} symmetry that involves the out-of-plane vibration of sp^3 carbon atoms (Li et al., 2020a; Irmer and Dorner-Reisel, 2005). While the G-band involves symmetric stretching of the C–C bonds and corresponds to first-order scattering of the stretching vibration mode (E_{2g}) reported for sp^2 hybridized carbon atoms in a hexagonal lattice of graphite layer (Mohan and Manoj, 2012; Han et al., 2012).

The intensity of peak D (I_D) reflects irregular crystal structures, whereas the intensity of peak G (I_G) expresses the regular crystal structures. Calculating the I_D/I_G ratio is essentially indicative of the proportionate number of defects in structure found in the graphene sheets of AC samples that have been synthesized. The I_D/I_G ratio values acquired for the rCB-based activated carbons exhibited a range of 1.037–1.223. Since the ID/IG ratio is more than 1, it indicates that there are a significant number of irregularities in AC crystal structures that can

Table 3
Ultimate analysis of rCB/ACs.

Sample	Yield content [wt.%]	C [wt.%]	H [wt.%]	N [wt.%]	S [wt.%]	O[a] [wt.%]
rCB	–	92.53	1.16	0.42	0.71	5.18
AC-800K	91.6	85.64	0.31	0.34	0.31	13.40
AC-850K	86.3	84.62	0.27	0.72	0.28	14.11
AC-900K	77.9	83.76	0.18	0.90	0.23	14.93
AC-500A	55.8	83.46	0.53	0.43	0.80	14.78
AC-600A	42.4	83.54	0.40	0.40	0.74	14.92
AC-700A	35.9	83.81	0.30	0.34	0.53	15.02

[a] It is obtained by calculation.

affect their physical and chemical properties. In general, higher crystallinity in materials can enhance CO_2 adsorption capacity due to improved stability and ordered arrangements, as well as the presence of well-defined pores or channels for CO_2 interaction (Nandi and Uyama, 2014). However, defects in crystalline materials, such as dislocations or vacancies, can also introduce additional adsorption sites, increasing the surface area available for CO_2 adsorption (Zhang et al., 2020). Both crystallinity and defects can influence CO_2 capture properties, with a balance between the two factors playing a crucial role in determining the overall adsorption performance. The higher increase in I_D/I_G is observed for physical activation, suggesting that it has resulted in the emergence of a greater number of defects in samples than utilizing KOH.

3.5. *Ultimate and proximate analysis*

The ultimate analysis (CHNS/O) of activated carbons at various activation temperatures is summarized in Table 3. The material in its pristine form showed a significant proportion of carbon (92.53 wt%) and a low content of other elements and ash (7.47 wt%), suggesting an astonishingly pure form of carbon. Chemically, the rCB/ACs produced using KOH generally exhibited a lower O content than those produced physically using air. The observed phenomenon can be attributed to the incorporation of oxygen-containing functional groups onto the surface of carbon. Moreover, the oxygen concentration of the ACs revealed a positive correlation with the activation temperature, whereby AC-900K demonstrates the highest value of 14.93 wt%. The determination of potassium content was also conducted using the XRF method. All samples of activated carbon by KOH contained small amounts of potassium, with concentrations not exceeding 0.09 wt%. The presence of K residues is likely to be attributed to their intercalation into the AC matrix and does not have a direct impact on CO_2 adsorption. On the other hand, physically activated carbons have contents ranging from 11.73 wt% to 33.92 wt%, with AC-700A possessing the highest record, likely due to significant oxidation during the activation process (Ahmadpour and Do, 1997). Additionally, physical activation with air resulted in sample degradation, which is a cause of the lowest carbon content that vaporizes while other minerals remain (Ogungbenro et al., 2018). In terms of other elements examined, AC-900K had the highest nitrogen content of 0.90 wt%. The sulphur content was very low (less than 1%) in all AC samples, indicating that no activation process introduced significant sulphur-containing functional groups, which can negatively impact the sorption performance of the material.

Table 4
Proximate analysis of rCB/ACs.

Sample	Volatile matter [wt.%]	Fixed carbon [wt.%]	Ash [wt.%]
rCB	0.56	91.12	8.32
AC-800K	1.86	88.34	9.80
AC-850K	2.04	87.07	10.89
AC-900K	2.12	86.64	11.24
AC-500A	0.75	89.80	9.45
AC-600A	0.70	88.94	10.36
AC-700A	0.90	86.50	12.60

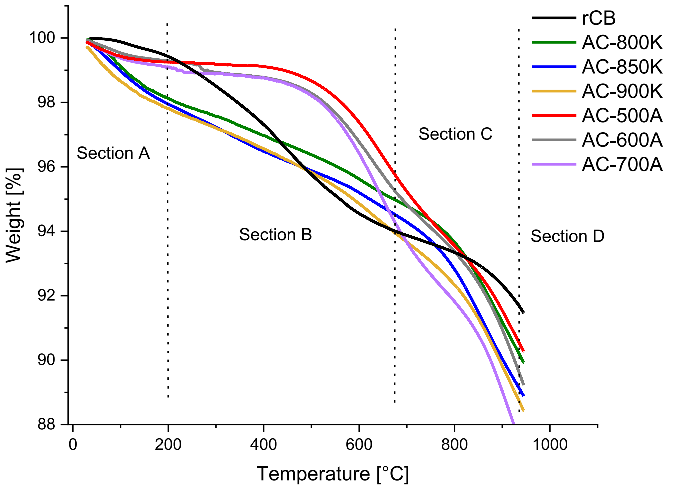

Fig. 9. Thermogravimetric analysis curves of rCB/AC samples.

The determination of activated carbon yield typically involves calculating the weight of activated carbon obtained after the activation and washing processes, and then dividing it by the starting weight of the unprocessed raw material. The yield content was in the range of 88.6–77.9%, and 55.8–35.9%, for chemically and physically produced ACs, indicating the high influence of air on burning off carbon. This calculation is performed on a dry basis, as outlined below:

$$\text{Yield content } [\%] = \frac{m_P}{m_{RM}} \bullet 100 \qquad (7)$$

Where: the variables m_P and m_{RM} represent the dry mass of the resulting AC (in grams) and the dry mass of the AC precursor (in grams).

Lastly, the proximate analysis results of the ACs are presented in Table 4. The volatile matter, fixed carbon, and ash content for all ACs samples varied within the range of 0.90–2.12, 86.50–89.90, and 9.45–12.60 wt%, respectively. The presented data indicates that the AC samples possess a comparatively high concentration of fixed carbon, making it suitable for various adsorption applications.

3.6. *Thermogravimetric analysis (TGA)*

The thermogravimetric analysis (TGA) curves of activated carbons up to 950 °C are presented in Fig. 9, showing three inflection points defining four distinct ranges for mass loss. Upon activation by air, the samples exhibited a weight loss of 0.71% at temperatures up to 200 °C, 4.46% within the temperature range of 200–700 °C, and 5.60% at temperatures exceeding 700 °C. The activation process utilizing KOH resulted in losses, approximately of 2.05%, 3.66%, and 5.34% wt. for temperatures below 200 °C, ranging from 200 to 700 °C, and higher than 700 °C, respectively.

The shape of the TGA profile is contingent upon the thermal behavior of the precursor, which is intrinsically linked to the chemical composition and chemical bonding present within the material structure. The reduction in mass in Section A can be attributed to the elimination of moisture or highly volatile compounds. Their removal is highly important, as it affects its physical and chemical properties, such as porosity and surface area (Sait et al., 2012). Furthermore, the substantial decrease in weight observed in Section B implies the removing of mineral matters along with the inorganic residues of ACs (Devi and Saroha, 2015), especially for physical activated samples, where the TGA curve

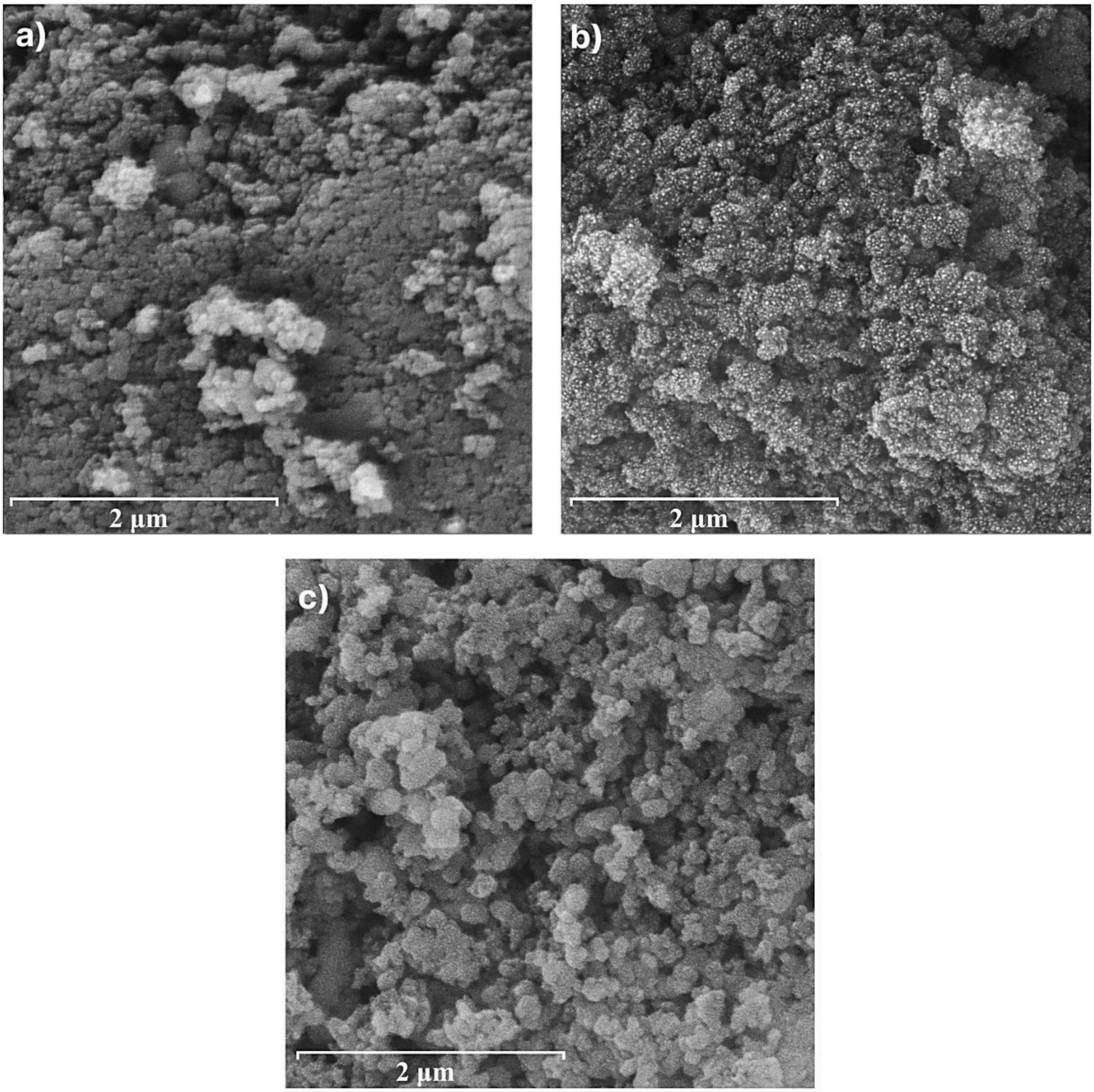

Fig. 10. SEM micrographs with a magnification of 52,000X at a resolution of 2 μm for (a) AC-700A, (b) AC-900K, and (c) recovered carbon black.

drastically decreased between 500 and 700 °C by more than 4.56%. In the third region (Section C), the gradual drop in the TGA curve indicates the combustion of the AC samples (Thonglhueng et al., 2022). The weight loss percentage in this section is relatively low, indicating that ACs have a high degree of purity and thermal stability in higher temperatures. The thermal gravimetric analysis (TGA) curve presented in this section can provide insight into the extent of carbonization of activated carbon and the thermal robustness of the recovered carbon black. Finally, in the fourth region (Section D), a small amount of ash residue (6–7%) was observed, suggesting the presence of inorganic components in samples after complete combustion at 930 °C.

3.7. Scanning electron microscopy (SEM) with energy-dispersive X-ray spectroscopy analysis (EDS)

Scanning electron microscopy with an energy-dispersive X-ray spectroscopy technique was applied to indicate details on the morphology and identify elements present on the surface of ACs along with their relative abundance. Fig. 10 presents the morphology with a magnification of 52,000X at a resolution of 2 μm for AC-700A and AC-900K that showed the most prominent textural properties, compared to the pristine recovered carbon black. In addition, more SEM images with varying magnification levels (ranging from 1000 to 7,000X) obtained at 20 μm and 100 μm, are given in Figure S2.

The complexity of activated carbons, in terms of composition and structure, surpasses that of rCB derived from waste tire pyrolysis. Based on SEM micrographs of synthesized ACs, the presence of porous and highly complex irregular structures differing in size and shape was confirmed, demonstrating a significant surface area beneficial to adsorption. The size, form, and surface attachments of the ACs are highly varied as a direct result of the elevated activation temperature effects. The ACs structure consisted of aggregates and agglomerates characterized by predominantly different-structured particles, while the macropores were dimly observable. Moreover, the observation of aggregates and agglomerates implies that the distribution of AC particles is non-uniform and instead forms clusters or larger groups, which may have an impact on the material's overall porous characteristics (Sun et al., 2016). Whereby, the particles do not possess constant shapes but instead exhibit variations and irregularities in their morphology, spherical or ellipsoidal in appearance (Fig. 11).

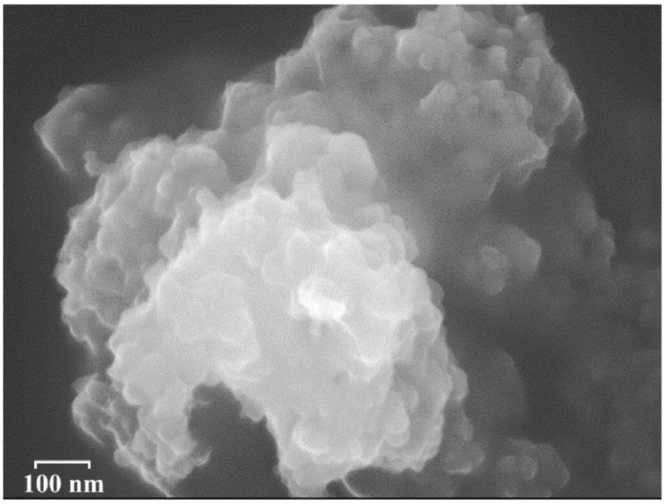

Fig. 11. SEM micrographs with a magnification of 50,000X at a resolution of 100 nm for rCB/ACs clusters.

s. The potential morphological changes occurring during the production of ACs based on recovered carbon black are schematically presented in Fig. 12.

Further, the EDS analysis has verified the atomic percentage of each composition in the sample. The element mapping images for AC-900K micrograph with a magnification of 7,000X at a resolution of 2 μm are depicted in Fig. 13(a–g). They demonstrate that the surface architecture of AC-900K predominantly comprises of carbon (C), oxygen (O) and potassium (K). Additionally, K residue compound refers to leftover potassium compounds from KOH, thus providing further confirmation that it may still be present in the activated carbon product, as was proved in elemental analysis. In contrast, the surface of activated carbon produced by physical activation using air (AC-700A) consists mainly of C, O, given in Fig. 14(a–g). Additionally, the small presence of silicon (Si), aluminum (Al), magnesium (Mg), and sulphur (S) was found, suggesting that additives may have been present in the initial recovered carbon black material, as highlighted in Section 2.1.

3.8. CO_2 adsorption investigation

The most promising samples from each activation type set were measured at four distinct temperatures, 0 °C, 15 °C, 25 °C and 30 °C under a pressure of 1 bar. As can be observed from the empirical data presented in Fig. 15, all curves exhibit an upward convex shape, which aligns with the Type-I (b) classification as defined by the International Union of Pure and Applied Chemistry (IUPAC) (Merin et al., 2021). Furthermore, the isotherm system indicates that the process was facile at low concentrations of CO_2, where a considerable proportion of the adsorption sites remain unoccupied by the gaseous molecules. Therefore, as the pressure increases, serving as the driving force, it led to an increase in the surface coverage of AC by intensifying CO_2 particles accumulation (Raganati et al., 2014). On the other hand, a rise in temperature caused a boost of the diffusion rate due to the heightened energy of gas molecules and also triggers instability of the adsorbed gas on the adsorbent surface, resulting in lower CO_2 adsorption capacities and making the process thermodynamically favorable at reduced temperatures. Gas molecules that are adsorbed possessed adequate energy to surpass the attractive forces present across the surface, thereby disrupting the surface bonds and relocating back into the gas phase, corresponding to the exothermic characteristic of adsorption (David and Kopac, 2014). Hence, it can be concluded that the process of CO_2 adsorption onto carbon-black derived activated carbons was primarily influenced by physisorption, which is driven by weak van der Waals forces that diminish as the temperature elevates. This statement is consistent with the principles outlined by Le Chatelier (Hendricks, 1941).

The AC-900K sample exhibited the highest CO_2 uptake of 30.90 cm^3/g under a pressure of 1 bar at 0 °C, possessing exceptional gas capture attributes comparable to commercial activated carbons. At temperatures of 15 °C, 25 °C and 30 °C, the CO_2 adsorption capacity was measured to

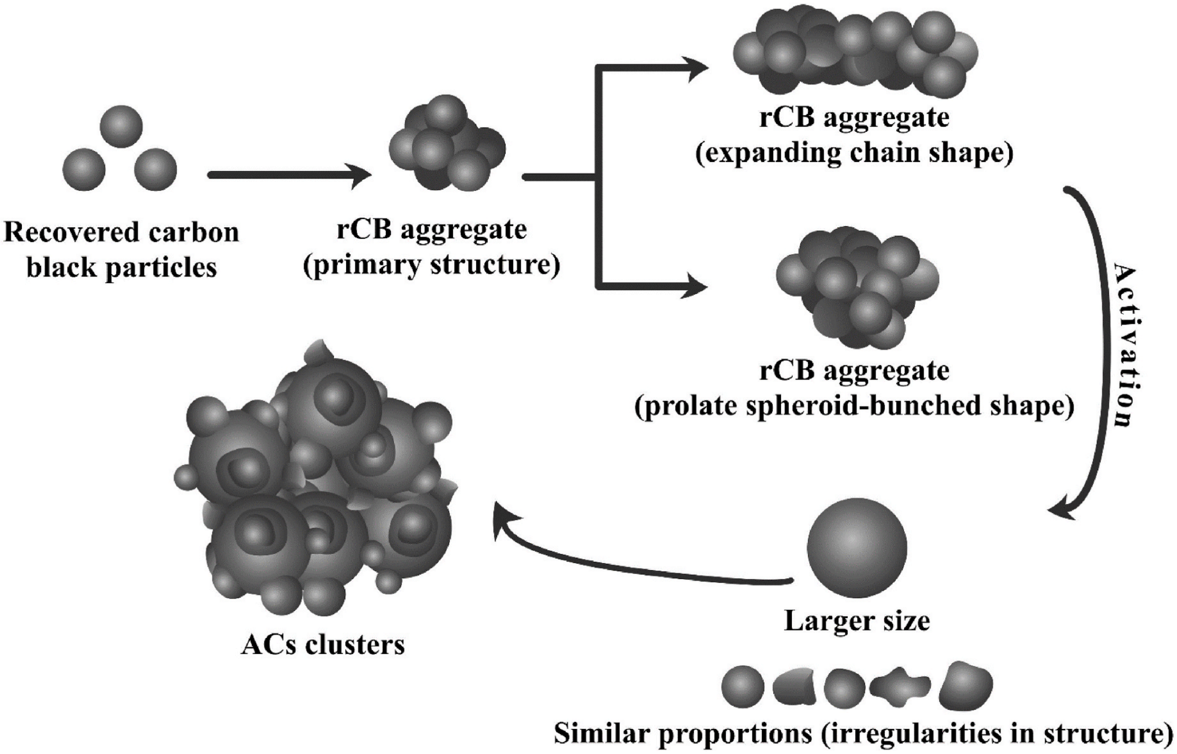

Fig. 12. Morphological changes of particles that occur during the activation process of recovered carbon black to activated carbons.

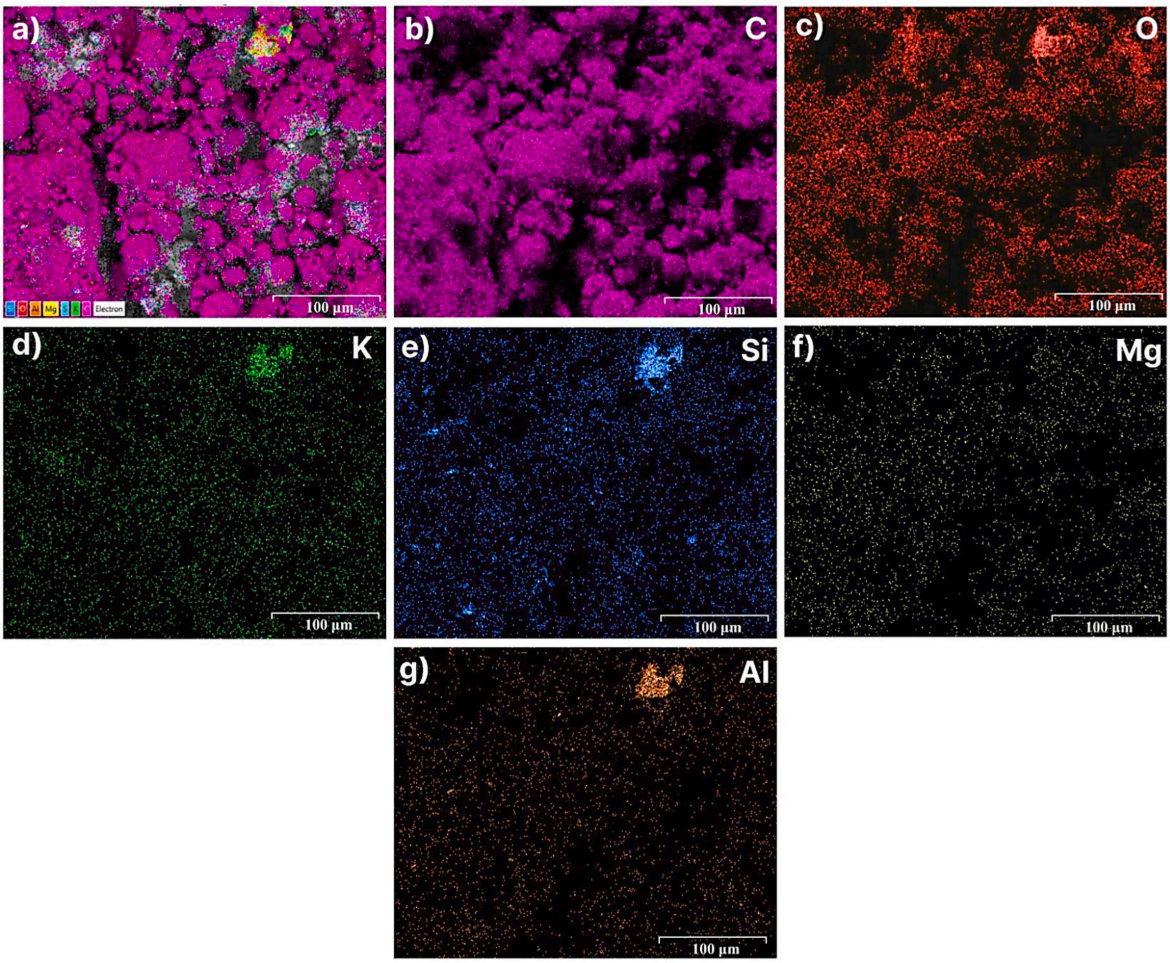

Fig. 13. Energy-dispersive X-ray spectroscopy analysis (EDS) of the AC-900K. (a) representative EDS image, and corresponding elemental mapping analysis: (b) C, (c) O, (d) K, (e) Si, (f) Mg, (g), Al.

be 24.75, 20.53, and 19.73 cm^3/g at the same pressure conditions. On the contrary, the AC-700A demonstrated a CO_2 adsorption capacity ranging from 14.79 to 22.56 cm^3/g at four temperatures under the pressure of 1 bar. Furthermore, for the rest of the samples obtained by chemical and physical activation CO_2 capacities were in the range of 22.39–15.99 cm^3/g at 0 °C, in the following order: AC-700A > AC-600A > AC-850K > AC-800K > AC-500A. It confirms that the optimal temperature for activation, with respect to CO_2 adsorption, was found to be 900 °C and 700 °C for potassium hydroxide and air, as activating agents.

Table 5 presents a summary of the findings obtained from CO_2 adsorption on activated carbons that were previously reported in the literature. The CO_2 uptake of recovered carbon black achieved in this work remain potentially competitive compared to other industrial byproducts, but they may not outperform ACs derived directly from biomass waste. As such, more research needs to focus their efforts and resources on exploring and harnessing the potential of rCB as a valuable resource for developing effective CO_2 adsorption solutions.

3.8.1. Influence of textural parameters on CO_2 adsorption

Additionally, to fully examine the correlation of adsorption with regard to textural properties, the dependance of all ACs obtained from rCB for CO_2 capture was evaluated at 0 °C. In order to achieve this objective, we ascertained the correlation between the adsorption of CO_2 and various textural parameters, namely the overall BET surface area (Fig. 16a), the total pore volume (Fig. 16b), the micropore volume with a width of <2 nm determined by the N_2 isotherm (Fig. 16c), and finally the volume of micropores with a width range below 1 nm determined by the CO_2 isotherm (Fig. 16d). The statistical measure known as the coefficient of determination (R^2) serves as a valuable tool to quantify the extent to which the independent variable can forecast the variance in the dependent variable (Wei et al., 2018). By analyzing the R^2 values, conclusions can be drawn about the influence of the texture characteristics on CO_2 adsorption. A high R^2 signifies a robust correlation, implying that the aforementioned factors have a notable impact on forecasting or elucidating the fluctuations in CO_2 adsorption. On the contrary, a diminishing R^2 value signifies a lack of relationship, thereby indicating its marginal impact on the observed variations (Burner et al., 2020).

The unambiguous interpretation of the coefficient of determination values was not readily apparent from the results of the examination due to its high values above 0.9. It may imply that the explication of the R^2 coefficients may not be straightforward. The analysis reveals that the R^2 values for chemical activation were the highest when examining the correlation between CO_2 uptake and the total pore volume or micropore volume determined by using CO_2 at 0 °C, suggesting that CO_2 adsorption mechanism was conditioned by them. Specifically, the R^2 values were equal to 0.946 and 0.940. For physical activation, adsorption mechanism was identified in relation to the specific surface area and micropore volume (determined through nitrogen adsorption) with the most significant values of the R^2 correlation coefficient, reaching 0.995 and 0.999. In summary, the analysis suggests that CO_2 sorption may be influenced by distinct factors associated with different activation methods. However, due to the high R^2 values, further analysis and interpretation may be necessary to fully understand the relationship

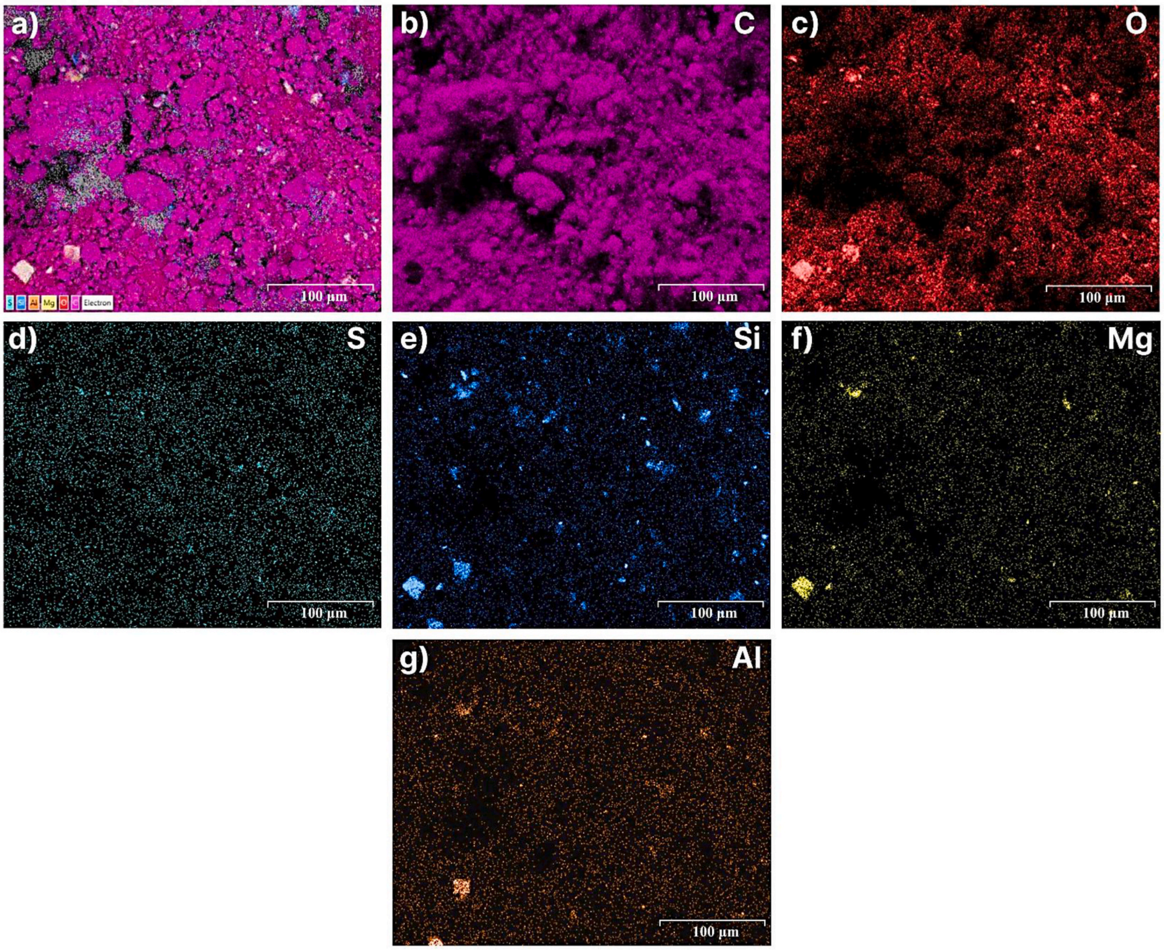

Fig. 14. Energy-dispersive X-ray spectroscopy analysis (EDS) of the AC-700A. (a) representative EDS image, and corresponding elemental mapping analysis: (b) C, (c) O.

between the independent variables and CO_2 capture in this context. Many studies reported similar cases (Serafin et al., 2022a, 2022b; Grundy and Ye, 2014), which would require evaluating especially the dependence of the R^2 on cumulative micropore volumes for particular pore diameter regions.

Fig. 17 illustrates the connection of coefficient of determination (R^2) in relation to the cumulative micropore volume within a specific range of pore width, ranging from 0.3 to 2 nm with a 0.1 nm increment (at 0 °C and up to 1 bar). The obtained results indicate that a pore micropores volumes varying from 0.30 to 0.40 nm exhibit the highest R^2 with an impressive value of 0.999, indicating an exceptionally strong positive correlation between CO_2 adsorption for each activation approach. Additionally, several three distinct pore ranges also demonstrate notable R^2 values (>0.9), specifically 0.6–0.7 nm, 0.7–0.8 nm, and 0.8–0.9 nm, for chemical activation. Regarding physical activation, the coefficient of determination demonstrated a comparable pattern within the corresponding pore range, such as: 0.4–0.5 nm, and 0.6–0.7 nm. The above observations mainly emphasize the significance of submicropores (<0.4 nm), ultramicropores (<0.7 nm) during CO_2 capture, thereby underscoring their vital function in the adsorption mechanism of rCB/ACs, which is schematically presented in Fig. 18.

3.8.2. Isotherm modeling studies

The application of mathematical isotherm modeling has been extensively used in order to elucidate the underlying fundamental mechanism involved in CO_2 capture process (Serafin and Dziejarski, 2023; Jagiello and Olivier, 2013; Jagiello et al., 2019a, 2019b). In this instance, five distinct three-parameter isotherms were selected based on their proven ability to accurately predict CO_2 adsorption, namely Toth, combined Freundlich-Langmuir, Sips, Redlich-Peterson, and Radke-Prausnitz.

A non-linear regression analysis was employed to model the CO_2 adsorption isotherms at 0, 5, 25 and 30 °C for the two samples that exhibited the superior CO_2 uptakes (AC-700A and AC-900K). To compare and contrast the precision of various equations, each model has been evaluated with the aim of minimizing an objective error function - the sum of absolute errors (EABS). The statistical procedure facilitated the identification of the isotherm model that displayed the lowest EABS values, indicating the minimized variance of distribution between the empirical and modelled data. The outcomes related to CO_2 adsorption on rCB/ACs are graphically shown in Fig. 19.

The study determined that the Freundlich-Langmuir equation is a dependable method for predicting CO_2 adsorption mechanism at four different temperatures for AC-900K. This conclusion was based on the observation of the smallest EABS obtained for all four CO_2-AC adsorption systems, ranging from 1.3965 to 4.393. Regarding the physically activated sample, specifically AC-700A, the most suitable model that correlated significantly effective with the experimental equilibrium adsorption data was the Redlich-Peterson, with EABS values that varied between 0.419 and 0.613. Furthermore, based on the maximum error functions observed in each dataset, it can be inferred that the Toth (EABS: 2.032–11.728), Sips (EABS: 2.5441–2.9349) equations are inadequate in providing a precise representation of the CO_2 sorption mechanism observed for AC-900K and AC-700A, respectively. To

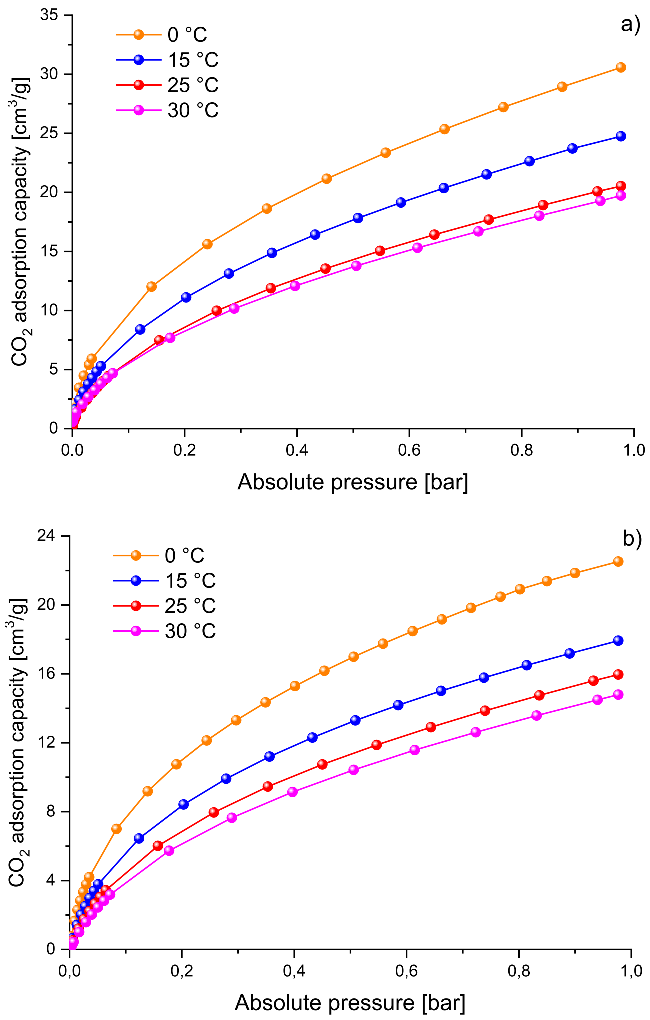

Fig. 15. The CO_2 adsorption isotherms at temperature of 0 °C, 15 °C, 25 °C, and 30 °C on (a) AC-900K and (b) AC-700A.

compare and contrast the fitting of the curves of the chosen isothermal models, their runs are shown for CO_2 adsorption in Figure S3.

The parameters of isotherm models that describe the best fit to the equilibrium CO_2 adsorption data for AC-900K and AC-700A are presented in Table 6. For the rest of the models all data is included in Table S1 and Table S2.

The interpretation of parameters for the most suitable models is another crucial step in accurately understanding the nature of adsorption on rCB/ACs surface. According to the Freundlich-Langmuir equation, it has been observed that an increase in sorption temperature leads to a reduction in the maximum adsorption capacity (q_m). Specifically, the q_m values decline from 418.0 cm^3/g at 0 °C to 114.5 cm^3/g at 30 °C. On the contrary, the K_{FL} constant exhibits a rise along with the temperature, confirming the exothermic nature of the CO_2 capture process. Moreover, for all CO_2-rCB/ACs systems, parameter n_{FL} is consistently lower than 1, which corresponds with the surface heterogeneity characteristic of ACs. With respect to the sample AC-700A, K_{RP} constant and the α_{RP} parameter of the Redlich-Peterson model demonstrate a similar correlation with the temperature as well as for the AC-900K. At 0 °C K_{RP} and α_{RP} are 300.9 $cm^3\ g^{-1}\cdot bar^{-1}$ and 12.16 $bar^{-\beta RP}$, while at 30 °C their values are reduced to 86.6 $cm^3\ g^{-1}\cdot bar^{-1}$ and 4.8 $bar^{-\beta RP}$, respectively. Finally, the β_{RP} exponent is almost constant throughout the range of 0.59–0.62, also indicating the adsorption on energetically heterogeneous surface.

Table 5
Comparison of CO_2 uptake of ACs derived from various waste at 1 bar and 25 °C for 100 vol% CO_2 feed.

AC precursor	Activation approach	CO_2 uptake (cm^3/g)	Reference
Global industrial waste			
Fly ash	KOH activation	13.44	Alhamed et al. (2015)
Polyacrylonitrile	KOH activation	17.02	Bai et al. (2015)
PET bottles	KOH activation	24.42	Arenillas et al. (2005)
Packaging waste	KOH activation	94.98	Idrees et al. (2018)
Charcoal	–	26.88	Lahuri et al. (2020)
Recovered carbon black	Air activation	16.00	This work
Recovered carbon black	KOH activation	20.53	This work
Biomass waste			
Rice husk	KOH activation	83.10	Li et al. (2015)
Palm shell charcoal	Steam activation	9.16	Khalil et al. (2012)
Rice husk	$ZnCl_2$ activation	29.12	Boonpoke et al. (2011)
Whitewood	Steam activation	30.01	Shahkarami et al. (2015)
Soybean factory waste	$ZnCl_2$ with CO_2 activation	20.83	Thote et al. (2010)
Common polypody	KOH activation	127.01	Serafin et al. (2022a)
Walnut shell	KOH activation	115.81	Serafin et al. (2023b)
Argan fruit shell	KOH activation	126.11	Boujibar et al. (2018)
Bee-collected pollen	KOH activation	72.71	Choi et al. (2019)
Empty fruit bunch	KOH activation	83.10	Parshetti et al. (2015)
Starch	KOH activation	86.02	Alabadi et al. (2015)

3.8.3. *Thermodynamic analysis*

Besides of the modeling of isotherms, it is crucial to examine the thermodynamic aspects of the interaction between AC and CO_2. The aim of this study was to gain a comprehensive understanding of the thermodynamic processes involved in the adsorption of CO_2 on activated carbon in a state of equilibrium. To verify the assumptions obtained from the analyzed isotherm models, changes in the Gibbs free energy (ΔG°), enthalpy (ΔH°), and entropy (ΔS°) of adsorption were identified. ΔH° and ΔS° were calculated from the van't Hoff equation in the form of a linear relationship ($ln(K_L)$ vs 1/T), as follows:

$$ln(K_L) = \frac{\Delta S^\circ}{R} - \frac{\Delta H^\circ}{RT} \tag{8}$$

where R is the universal gas constant (8.314 J/mol·K), K_L is the Langmuir adsorption constant that has been utilized as the conventional thermodynamic equilibrium indicator for the computation of thermodynamic parameters [1/bar], and T is absolute temperature [K].

Whereas ΔG° was estimated from the below equation by using Langmuir constant:

$$\Delta G^\circ = -RT\ ln(K_L) \tag{9}$$

Table 7 presents the thermodynamic parameters that were derived from Eq. (7) and Eq. (8). The analysis of their values reveals that changes in standard free entropy and enthalpy remain unaffected by variations in the adsorption temperature. Furthermore, their negative numerical values ($\Delta S^\circ<0$, $\Delta H^\circ<0$) indicate a reduction in disorder and randomness of the CO_2-rCB/AC system and the degree of freedom of CO_2, along with the exothermic nature of adsorption (Abel et al., 2020; Abunowara et al., 2023). This can be attributed to the formation of attractive forces between the rCB/AC surface and CO_2 molecules, leading to their accumulation. In addition, the standard enthalpy change is less than 40 kJ/mol, which suggest physisorption (Ashraf et al., 2022), confirming

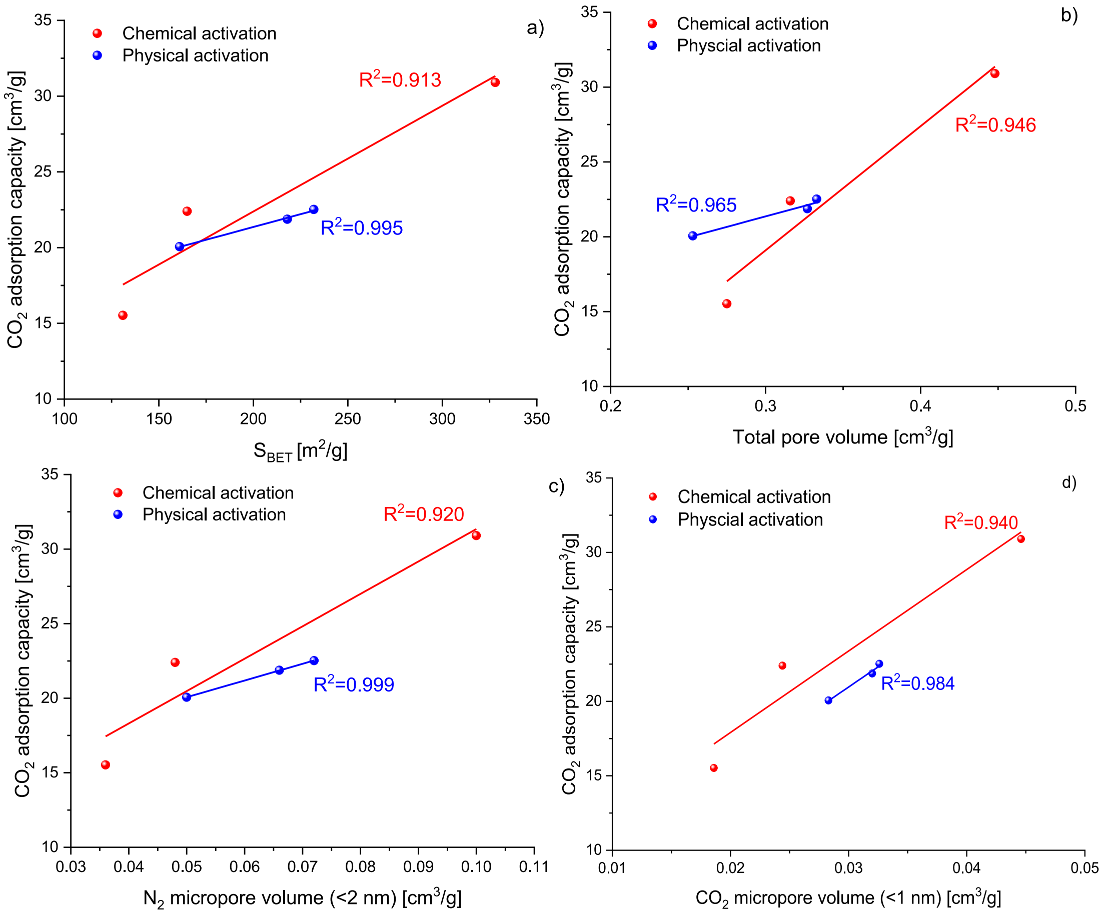

Fig. 16. CO_2 adsorption uptake at 0 °C up to 1 bar as a function of (a) BET surface area (b) total pore volume (c) N_2 micropore volume <2 nm and (d) CO_2 micropore volume <1 nm.

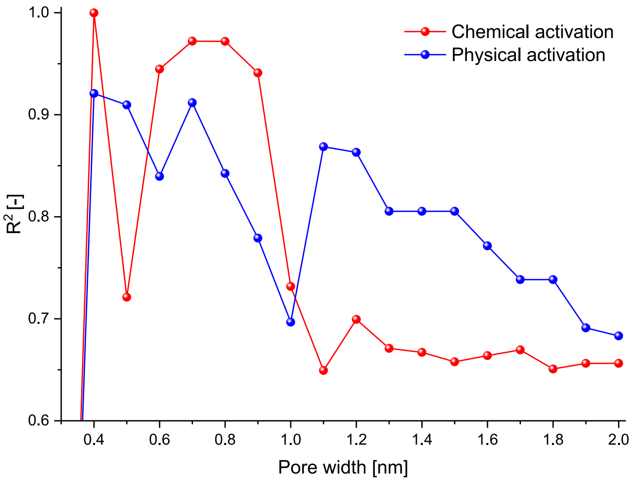

Fig. 17. Relationship between the coefficient of determination and cumulative pore volume within the range of 0.3–2 nm, at 0 °C under a pressure of 1 bar.

the assumptions of the isotherm models. The spontaneous character of the process may also be deduced from the fact that the change in ΔG° exhibits negative values. The estimation of ΔG° via Eq. (8) yields insights into the increased favorable binding of CO_2 molecules at lower temperatures, as a reduction in the negative value of ΔG° is observed as the temperature increases (Du et al., 2021). The performed thermodynamic analysis validated prior findings regarding the characteristics of adsorption. Specifically, it showed that high temperatures lead to a reduction in the strength of the bonds between the adsorbate and the adsorbent, which consequently causes the desorption of the CO_2 molecules. When comparing thermodynamic parameters for physically and chemically activated carbons, the results suggest that the adsorption process is more energetically and entropically favorable for AC-900K than AC-700A.

Furthermore, the fundamental focus of thermodynamic investigation related to surface phenomena involves the mathematical representation of isosteric heat of adsorption. This particular variable serves as a clear indicator of interaction strength between adsorbate and the adsorbent surface, referring to the thermal energy produced during the CO_2 capture process (Serafin et al., 2019), as given by the Clausius-Clapeyron equation:

$$Q_{st} = -R\left(\frac{\partial(\ln(p))}{\partial\left(\frac{1}{T}\right)}\right)_{\theta} \tag{10}$$

where: p is the partial pressure of the CO_2 at equilibrium state [bar], T is absolute temperature [K], R is the ideal gas constant [J/mol·K], Q_{st} denotes isosteric heat of adsorption [J/mol], and θ indicates a specific surface coverage [-].

The pressure values for the specified surface covering degree have been determined using the rearranged Langmuir-Freundlich isotherm equation for AC-900K that efficiently characterized the CO_2 adsorption

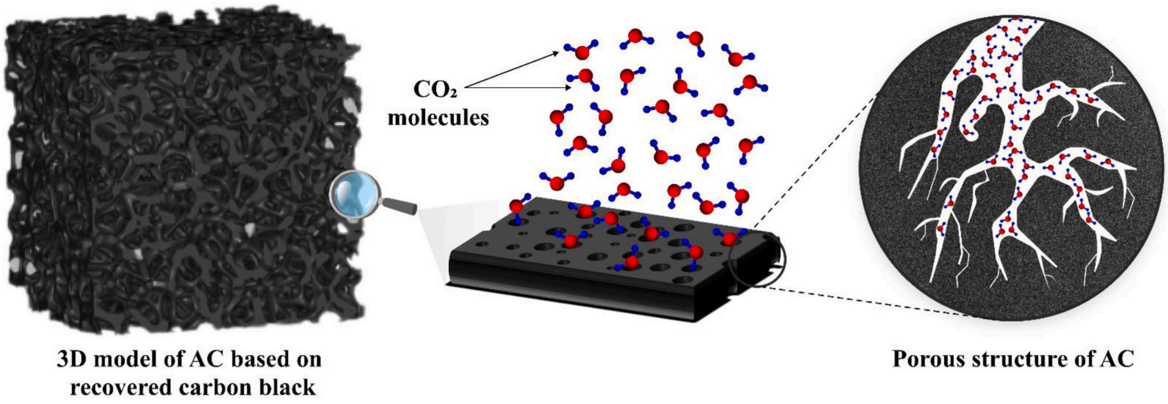

Fig. 18. A schematic representation of the CO_2 adsorption mechanism on AC based on recovered carbon black.

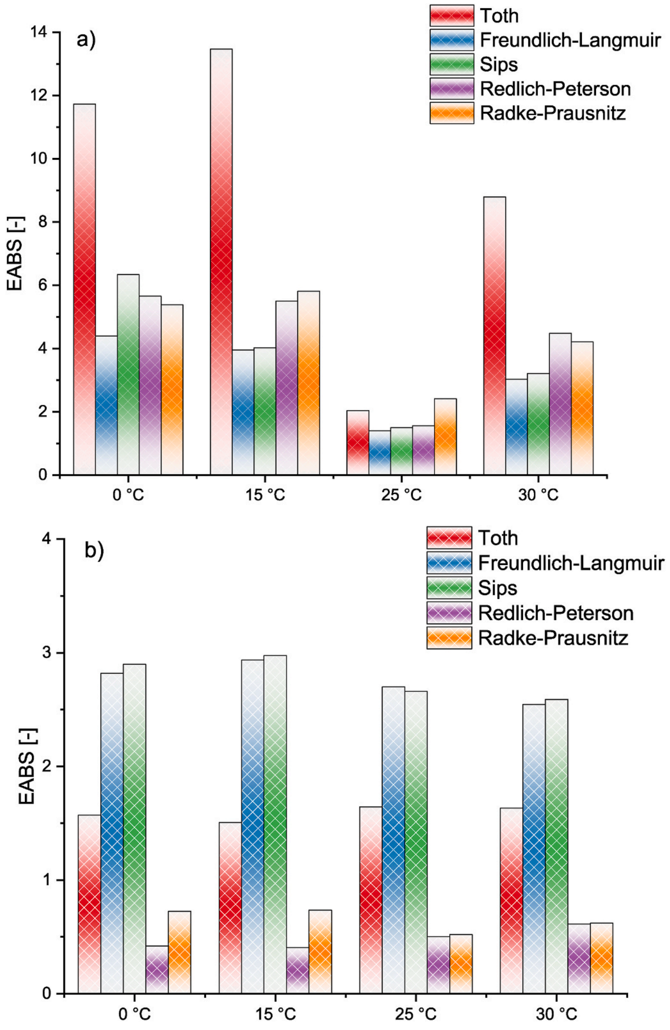

Fig. 19. Summarization of EABS values obtained through data fitting of chosen isotherm models by non-linear regression for (a) AC-900K and (b) AC-700A.

process:

$$p(n) = \sqrt[n_{FL}]{\frac{q_e}{q_m \bullet K_{FL} - q_e \bullet K_{FL}}} \tag{11}$$

The same approach was also applied for AC-700A by implementing the Redlich-Peterson isotherm model.

Table 6
Parameters for the best fitted isotherm model to the experimental data.

Temperature	0 °C	15 °C	25 °C	30 °C
Model	Freundlich-Langmuir[a]			
q_m [cm^3/g]	418.020	232.930	115.947	114.500
K_{FL} [bar^{-nFL}]	0.0799	0.121	0.207	0.218
n_{FL} [-]	0.511	0.556	0.630	0.603
Model	**Redlich-Peterson**[b]			
K_{RP} [$cm^3 \cdot g^{-1} \cdot bar^{-1}$]	300.937	172.845	116.110	86.5821
α_{RP} [$bar^{-\beta RP}$]	12.156	8.552	6.194	4.789
β_{RP} [-]	0.622	0.622	0.594	0.596

[a] The best fitted isotherm model for AC-900K.
[b] The best fitted isotherm model for AC-700A.

Finally, thirty points of CO_2 adsorbed amount were used to determine the absolute pressure at each temperature and then to calculate the slope of the straight lines from the data sets of ln(p) versus T^{-1}. The isosteric heat of adsorption as a function of surface coverage (θ) on ACs is presented in Fig. 20.

The range of isosteric heat of adsorption was found to be within the range of 15.19–27.51 kJ/mol and 22.28–36.81 kJ/mol in relation to the total surface coverage for AC-700A and AC-900K, respectively. These data provide solid confirmation that the CO_2 sorption occurring in activated carbons is of a physical nature that is controlled by relatively weak van der Waals forces. Physical adsorption has a modest Q_{st}, which differs from 20 to 40 kJ/mol, while the heat of chemisorption generally falls into the range of 80–200 kJ/mol (Li et al., 2020b). Comparable outcomes have been attained by Tang et al. (2023) and Guo et al. (2020).

Additionally, according to reported research, it has been determined that easily regenerable solid sorbents used for CO_2 capture application must exhibit a preferable heat of adsorption that falls between 26 and 31 kJ/mol for a 20% partial pressure CO_2 flue gas and 22–28 kJ/mol for single-component CO_2 streams (Mert et al., 2023). The present study shows that the isosteric heat of the CO_2 adsorption values of activated carbons meets these specified criteria. Further, the obtained results indicate that there is a significant increase in Qst values at a lower surface coverage, followed by a gradual decline along with a higher degree of surface coverage. There are several possible reasons for this phenomenon, including cooperative effects (Nazir et al., 2021), molecular rearrangement (Guclu et al., 2021), or, especially, the saturation effect. Initially, at lower θ the active adsorption sites are available and it is easier for the CO_2 molecules to interact with these sites, which results in higher adsorbent-adsorbate interactions and thus higher Qst values. Therefore, as the surface coverage of the AC increases, the available strong adsorption sites become progressively occupied, leading to a decrease in the strength of interaction between CO_2 molecules and the remaining vacant sites on the surface.

Table 7
Thermodynamic parameters of CO_2 adsorption.

	AC-900K			AC-700A		
T [°C]	ΔG^0 [kJ/mol]	ΔS^0 [kJ/mol·K]	ΔH^0 [kJ/mol]	ΔG^0 [kJ/mol]	ΔS^0 [kJ/mol·K]	ΔH^0 [kJ/mol]
0	−2.027	−0.0240	−8.626	−2.534	−0.0365	−12.540
15	−1.772			−2.136		
25	−1.601			−1.736		
30	−1.209			−1.387		

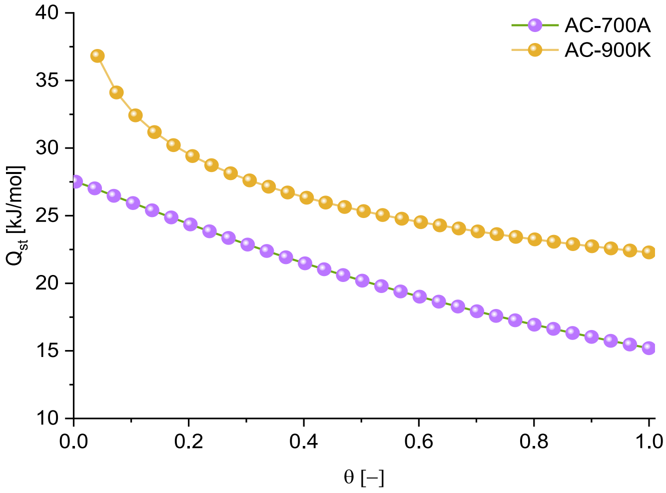

Fig. 20. The isosteric heat of adsorption as a function of surface coverage for AC-900K and AC-700A.

3.8.4. *Insights into CO_2/N_2 selectivity*

Selectivity adsorption of CO_2 over N_2 is an important factor that should be considered, when assessing adsorbents for the purpose of CO_2 removal from flue gas in carbon capture technologies. Hence, the AC-700A and AC-900K samples, exhibiting the highest CO_2 adsorption capacity, were subjected to nitrogen adsorption measurement at a temperature of 25 °C and a pressure of 1 bar. The results of N_2 adsorption studies are shown in Figure S4.

The Myers and Prausnitz's ideal adsorbed solution theory (IAST) (Gharagheizi and Sholl, 2021) is a commonly employed method for the estimation of adsorption selectivity and mixed-gas adsorption isotherms based on pure-component isotherms. This approach has been found to yield accurate results for a diverse range of systems. The present study utilized IAST to forecast the selectivity of CO_2 over N_2 by relying on the individual adsorption isotherms of these gases

$$S_{IAST} = \frac{q_{CO_2(p)}}{q_{N_2(p)}} \bullet \frac{p_{N_2}}{p_{CO_2}} \tag{12}$$

where: S_{IAST} is the selectivity coefficient, $q_{CO2(p)}$ and $q_{N2(p)}$ refer to the uptake of specific gas [cm^3/g], p_{N2} and p_{CO2} are the partial pressure in the mixture.

Therefore, the selectivity for an equimolar CO_2 and N_2 binary mixture ($S_{IAST(EQM)}$) was analyzed, with equation (11) being expressed as follows:

$$S_{IAST(EQM)} = \frac{q_{CO_{2(p)}}}{q_{N_{2(p)}}} \tag{13}$$

where: $q_{i(p)}$ is the adsorption capacity [cm^3/g] at the same partial pressure p of CO_2 and N_2.

Further, it is of great significance to evaluate the selectivity with regards to flue gas compositions that correspond to those discharged directly from the industrial sector. It is widely acknowledged that the flue gases generated by the most established CO_2 capture technique,

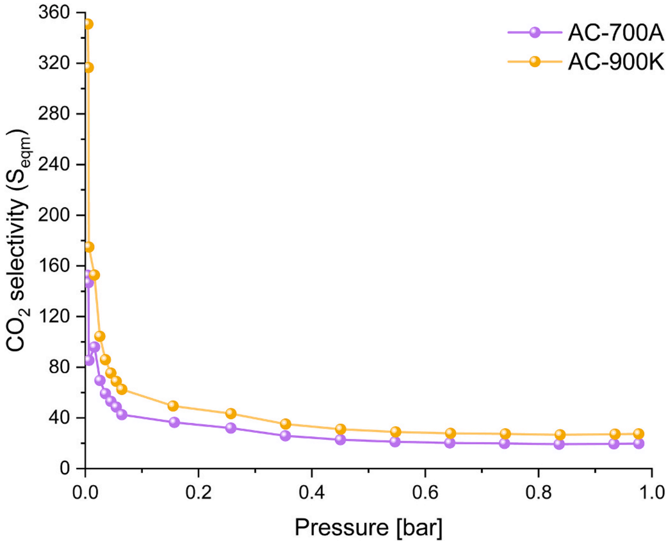

Fig. 21. IAST selectivity for CO_2 over N_2 at 25 °C for a CO_2/N_2 binary mixture.

namely post-combustion capture, generally comprise approximately 10–15% CO_2 and 75–80% N_2, in addition to other gases including oxygen, carbon monoxide, and sulphur dioxide. Therefore, selectivity for flue gas composition ($S_{IAST(FG)}$) equals 15% CO_2 and 85% N_2 was calculated also based on IAST method using the below equation:

$$S_{IAST(FG)} = \frac{q_{CO_2@0.15\ bar}}{q_{N_2@0.85\ bar}} \bullet \frac{0.85}{0.15} \tag{14}$$

where: $q_{i@jbar}$ is the adsorption capacity [cm^3/g] of CO_2 and N_2 at the partial pressure of 0.15 and 0.85 respectively.

Fig. 21 presents selectivity calculated using single component gas adsorption capacity for equimolar CO_2 and N_2 binary mixture. The selectivity ratio of CO_2 to N_2 was observed to decrease at a pressure of approximately 0.08 bar for the two activated carbon samples. The highest CO_2/N_2 selectivity coefficient at 0.001 bar was 164.80 and 350.91 for AC-700A and AC-900K. Subsequently, as the pressure increased, the selectivity coefficient exhibited a decreasing trend, ultimately attaining values of 19.77 and 27.39 at a pressure of 1 bar. In the case of a gaseous mixture comprising 15% CO_2 and 85% N_2, the CO_2/N_2 selectivity achieved 59.70 and 44.51 at a pressure of 1 bar, for AC-900K and AC-700A. The obtained values are significantly higher than those described in the literature (Serafin et al., 2022a).

3.8.5. *Cyclic regeneration stability*

The regeneration capacity of ACs is a significant aspect in determining the efficacy as an adsorbent material, directly influencing its lifespan and the overall economic feasibility of CO_2 capture process. This characteristic pertains to the inherent capability of ACs to undergo many adsorption-desorption regeneration cycles and regain its initial adsorption capacity subsequent to being fully saturated with adsorbate. Therefore, the stability potential of the AC-900K and AC-700A was evaluated by performing 1 st, 5 th, and 10 th adsorption-desorption runs

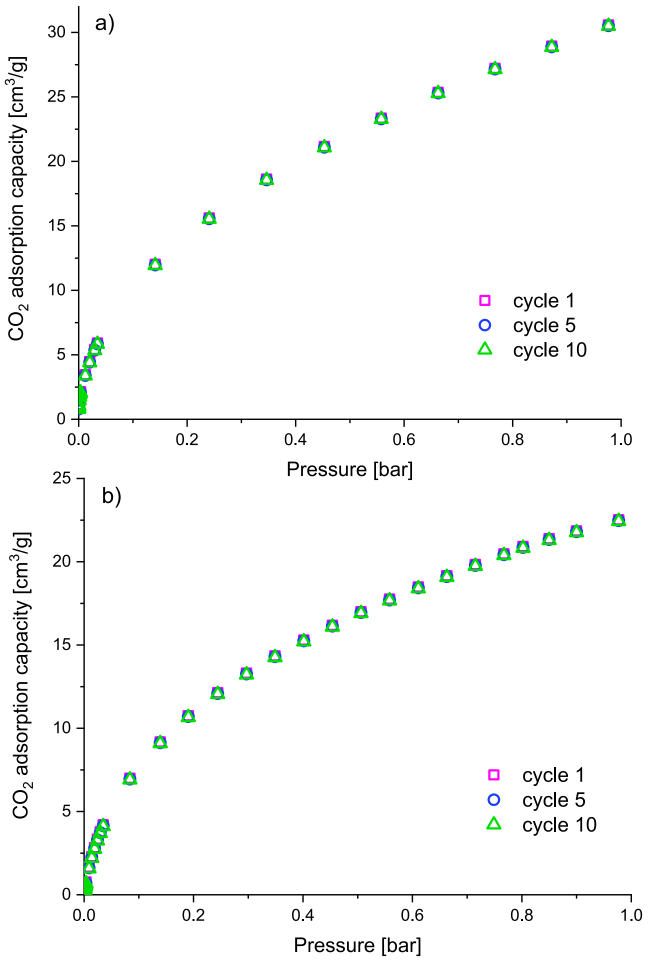

Fig. 22. CO_2 capture performance for (a) AC-900K -and (b) AC-700A at 0 °C in 1st, 5th, and 10th adsorption-desorption cycle.

at a temperature of 0 °C (Fig. 22). After a total of ten cycles, there were no observable differences in the CO_2 uptake performance. The maximum value of the standard deviation equaled 0.09, proving that rCB/ACs exhibits exceptional stability as a solid CO_2 adsorbent.

4. Conclusions

In this work, the high-value-added ACs derived from tailor-made rCB obtained through commercial-scale ELTs pyrolysis for CO_2 capture application have been characterized and reported for the first time in the literature.

The chemically activated carbon material via KOH at 900 °C (AC-900K) among all samples exhibited a notable development in specific surface area, total pore volume, and micropore volume compared to the pristine material that were found to be 328 m^2/g, 0.448 cm^3/g, and 0.100 cm^3/g, respectively. Furthermore, the AC-900K revealed a competitive CO_2 adsorption capacity to other ACs derived from industrial waste, with values of 30.90 cm^3/g at 0 °C and 20.53 cm^3/g at 25 °C under 1 bar, accordingly. The investigation of the CO_2 adsorption mechanism revealed that Freundlich-Langmuir and Redlich-Peterson models demonstrate a high degree of precision in predicting the adsorption behaviors of CO_2 on the AC surface, thus confirming the occurrence of multilayer sorption on the heterogeneous surface. The isosteric heat of adsorption was determined, resulting values suggest favorable application of those materials in CO_2 capture. Additionally, the selectivity of CO_2/N_2 was relatively high, achieving 350.91 and 59.70 for the binary mixture and composition of flue gases commonly encountered in post-combustion capture technology, respectively. Ultimately, rCB/ACs showed the superior cyclic regeneration over 10th cycles.

In general, this study investigates the potential for recycling rCB directly obtained from the industrial-scale pyrolysis of ELTs, which yields a valuable product in the form of ACs. While the CO_2 uptake of the prepared rCB/ACs may be limited to biomass-based ones, they exhibit performance comparable to numerous materials derived from global industrial by-products. On top of that, it is worth noting that the achievement of superior textural characteristics can be further accomplished through the optimization of activation parameters. Consequently, it is strongly advised that additional modification of the activation factors be undertaken to fully exploit the research path of rCB/ACs. Based on the investigations carried out, the final findings proved that the upgraded rCB/ACs developed exhibited further potential CO_2 capture capabilities. In overall, this research contributes to sustainable waste management practices on commercial scale, offering a green solution for repurposing globally discarded ELTs. This highly aligns with the principles of resource efficiency and responsible materials production.

CRediT authorship contribution statement

Bartosz Dziejarski: Conceptualization, Methodology, Experiment, Validation, Data curation, Formal analysis, Software, Investigation, Writing – original draft, Writing – review & editing, Visualization, Project administration. **Diego Felipe Hernández-Barreto:** Conceptualization, Methodology, Experiment, Modeling, Validation, Data curation, Formal analysis, Investigation, Writing – original draft, Writing – review & editing. **Juan Carlos Moreno-Piraján:** Conceptualization, Methodology, Investigation, Supervision, Resources, Funding acquisition. **Liliana Giraldo:** Conceptualization, Investigation, Supervision. **Jarosław Serafin:** Experiment, Formal analysis, Data curation. **Pavleta Knutsson:** Conceptualization, Investigation, Supervision. **Klas Andersson:** Investigation, Supervision. **Renata Krzyżyńska:** Investigation, Supervision.

Declaration of competing interest

The authors declare that they have no known competing financial interests or personal relationships that could have appeared to influence the work reported in this paper.

Data availability

No data was used for the research described in the article.

Acknowledgement

Bartosz Dziejarski extends his gratitude to Prof. Juan Carlos Moreno Piraján (Departamento de Química, Facultad de Ciencias, Grupo de Investigación en Sólidos Porosos y Calorimetría, Universidad de los Andes) and Prof. Liliana Giraldo (Departamento de Química, Grupo de Calorimetría, Universidad Nacional de Colombia) for their exceptional hospitality and for providing the invaluable opportunity to carry out research within their esteemed laboratory. Their collaborative spirit and dedication to fostering a stimulating research environment have been instrumental in presented paper. Prof. Dr. Juan Carlos Moreno-Piraján also acknowledges the Facultad de Ciencias of Universidad de los Andes for the grant (No. INV-2023-162-2735). Diego F. Hernández thanks to "Fondo de Apoyo Financiero para Doctorados" of Universidad de los Andes and to the Ministerio de Ciencia, Tecnología e Innovación for the financial support of the doctorate studies, by the "Convocatoria Nacional para Doctorados 909-2".

Appendix A. Supplementary data

Supplementary data to this article can be found online at https://doi.org/10.1016/j.envres.2024.118169.

References

Abel, U.A., Habor, G.R., Oseribho, O.I., 2020. Adsorption studies of oil spill clean-up using coconut coir activated carbon (CCAC). Am. J. Chem. Eng. 8 (2), 36–47. https://doi.org/10.11648/j.ajche.20200802.11.

Abuelnoor, N., AlHajaj, A., Khaleel, M., Vega, L.F., Abu-Zahra, M.R., 2021. Activated carbons from biomass-based sources for CO_2 capture applications. Chemosphere 282, 131111. https://doi.org/10.1016/j.chemosphere.2021.131111.

Abunowara, M., Bustam, M.A., Sufian, S., Babar, M., Eldemerdash, U., Mukhtar, A., Ullah, S., Assiri, M.A., Al-Sehemi, A.G., Lam, S.S., 2023. High pressure CO_2 adsorption onto Malaysian Mukah-Balingian coals: adsorption isotherms, thermodynamic and kinetic investigations. Environ. Res. 218, 114905 https://doi.org/10.1016/j.envres.2022.114905.

Ahmadpour, A., Do, D.D., 1997. The preparation of activated carbon from macadamia nutshell by chemical activation. Carbon 35 (12), 1723–1732. https://doi.org/10.1016/S0008-6223(97)00127-9.

Alabadi, A., Razzaque, S., Yang, Y., Chen, S., Tan, B., 2015. Highly porous activated carbon materials from carbonized biomass with high CO_2 capturing capacity. Chem. Eng. J. 281, 606–612. https://doi.org/10.1016/j.cej.2015.06.032.

Alhamed, Y.A., Rather, S.U., El-Shazly, A.H., Zaman, S.F., Daous, M.A., Al-Zahrani, A.A., 2015. Preparation of activated carbon from fly ash and its application for CO_2 capture. Kor. J. Chem. Eng. 32, 723–730. https://doi.org/10.1007/s11814-014-0273-2.

Aniruddha, R., Sreedhar, I., Reddy, B.M., 2020. MOFs in carbon capture-past, present and future. J. CO2 Util. 42, 101297 https://doi.org/10.1016/j.jcou.2020.101297.

Arenillas, A., Rubiera, F., Parra, J.B., Ania, C.O., Pis, J.J., 2005. Surface modification of low cost carbons for their application in the environmental protection. Appl. Surf. Sci. 252 (3), 619–624. Surface modification of low cost carbons for their application in the environmental protection. Applied Surface Science, 252(3), 619-624.

Arslanoğlu, H., 2019. Direct and facile synthesis of highly porous low cost carbon from potassium-rich wine stone and their application for high-performance removal. J. Hazard Mater. 374, 238–247. https://doi.org/10.1016/j.jhazmat.2019.04.042.

Ashraf, M.T., AlHammadi, A.A., El-Sherbeeny, A.M., Alhammadi, S., Al Zoubi, W., Ko, Y. G., Abukhadra, M.R., 2022. Synthesis of cellulose fibers/Zeolite-A nanocomposite as an environmental adsorbent for organic and inorganic selenium ions; Characterization and advanced equilibrium studies. J. Mol. Liq. 360, 119573 https://doi.org/10.1016/j.molliq.2022.119573.

Ayinla, R.T., Dennis, J.O., Zaid, H.M., Sanusi, Y.K., Usman, F., Adebayo, L.L., 2019. A review of technical advances of recent palm bio-waste conversion to activated carbon for energy storage. J. Clean. Prod. 229, 1427–1442. https://doi.org/10.1016/j.jclepro.2019.04.116.

Bai, B.C., Kim, E.A., Lee, C.W., Lee, Y.S., Im, J.S., 2015. Effects of surface chemical properties of activated carbon fibers modified by liquid oxidation for CO_2 adsorption. Appl. Surf. Sci. 353, 158–164. https://doi.org/10.1016/j.apsusc.2015.06.046.

Baldovino-Medrano, V.G., Niño-Celis, V., Isaacs Giraldo, R., 2023. Systematic analysis of the nitrogen adsorption–desorption isotherms recorded for a series of materials based on microporous–mesoporous amorphous aluminosilicates using classical methods. J. Chem. Eng. Data. https://doi.org/10.1021/acs.jced.3c00257.

Basik, A.A., Sanglier, J.J., Yeo, C.T., Sudesh, K., 2021. Microbial degradation of rubber: actinobacteria. Polymers 13 (12), 2021. https://doi.org/10.3390/polym13121989.

Bhattacharjya, D., Park, H.Y., Kim, M.S., Choi, H.S., Inamdar, S.N., Yu, J.S., 2014. Nitrogen-doped carbon nanoparticles by flame synthesis as anode material for rechargeable lithium-ion batteries. Langmuir 30 (1), 318–324. https://doi.org/10.1021/la403366e.

Boonpoke, A., Chiarakorn, S., Laosiripojana, N., Towprayoon, S., Chidthaisong, A., 2011. Synthesis of activated carbon and MCM-41 from bagasse and rice husk and their carbon dioxide adsorption capacity. Journal of Sustainable Energy & Environment 2 (2), 77–81.

Boujibar, O., Souikny, A., Ghamouss, F., Achak, O., Dahbi, M., Chafik, T., 2018. CO_2 capture using N-containing nanoporous activated carbon obtained from argan fruit shells. J. Environ. Chem. Eng. 6 (2), 1995–2002. https://doi.org/10.1016/j.jece.2018.03.005.

Boujibar, O., Ghamouss, F., Ghosh, A., Achak, O., Chafik, T., 2019. Activated carbon with exceptionally high surface area and tailored nanoporosity obtained from natural anthracite and its use in supercapacitors. J. Power Sources 436, 226882. https://doi.org/10.1016/j.jpowsour.2019.226882.

Brown, S.D.M., Jorio, A., Dresselhaus, M.S., Dresselhaus, G., 2001. Observations of the D-band feature in the Raman spectra of carbon nanotubes. Phys. Rev. B 64 (7), 073403. https://doi.org/10.1103/PhysRevB.64.073403.

Bulei, C., Todor, M.P., Heput, T., Kiss, I., 2018. Directions for material recovery of used tires and their use in the production of new products intended for the industry of civil construction and pavements. In: IOP Conference Series: Materials Science and Engineering. IOP Publishing, 012064. https://doi.org/10.1088/1757-899X/294/1/012064, 294, No. 1.

Burner, J., Schwiedrzik, L., Krykunov, M., Luo, J., Boyd, P.G., Woo, T.K., 2020. High-performing deep learning regression models for predicting low-pressure CO_2 adsorption properties of metal–organic frameworks. J. Phys. Chem. C 124 (51), 27996–28005. https://doi.org/10.1021/acs.jpcc.0c06334.

Cai, K., Liu, P., Zhao, T., Su, K., Yang, Y., Tao, D.J., 2022. Construction of hyper-crosslinked ionic polymers with high surface areas for effective CO_2 capture and conversion. Microporous Mesoporous Mater. 343, 112135 https://doi.org/10.1016/j.micromeso.2022.112135.

Cardona-Uribe, N., Betancur, M., Martínez, J.D., 2021. Towards the chemical upgrading of the recovered carbon black derived from pyrolysis of end-of-life tires. Sustainable Materials and Technologies 28, e00287. https://doi.org/10.1016/j.susmat.2021.e00287.

Choi, S.W., Tang, J., Pol, V.G., Lee, K.B., 2019. Pollen-derived porous carbon by KOH activation: effect of physicochemical structure on CO_2 adsorption. J. CO2 Util. 29, 146–155. https://doi.org/10.1016/j.jcou.2018.12.005.

Dabic-Miletic, S., Simic, V., Karagoz, S., 2021. End-of-life tire management: a critical review. Environ. Sci. Pollut. Control Ser. 1–18. https://doi.org/10.1007/s11356-021-16263-6.

Dantas, S., Struckhoff, K.C., Thommes, M., Neimark, A.V., 2019. Phase behavior and capillary condensation hysteresis of carbon dioxide in mesopores. Langmuir 35 (35), 11291–11298. https://doi.org/10.1021/acs.langmuir.9b01748.

David, E., Kopac, J., 2014. Activated carbons derived from residual biomass pyrolysis and their CO_2 adsorption capacity. J. Anal. Appl. Pyrol. 110, 322–332. https://doi.org/10.1016/j.jaap.2014.09.021.

Devi, P., Saroha, A.K., 2015. Effect of pyrolysis temperature on polycyclic aromatic hydrocarbons toxicity and sorption behaviour of biochars prepared by pyrolysis of paper mill effluent treatment plant sludge. Bioresour. Technol. 192, 312–320. https://doi.org/10.1016/j.biortech.2015.05.084.

Du, X., Pang, D., Cheng, Y., Zhao, Y., Hou, Z., Liu, Z., Wu, T., Shu, C., 2021. Adsorption of CH_4, N_2, CO_2, and their mixture on montmorillonite with implications for enhanced hydrocarbon extraction by gas injection. Appl. Clay Sci. 210, 106160 https://doi.org/10.1016/j.clay.2021.106160.

Dziejarski, B., Serafin, J., Andersson, K., Krzyżyńska, R., 2023. CO_2 capture materials: a review of current trends and future challenges. Materials Today Sustainability, 100483. https://doi.org/10.1016/j.mtsust.2023.100483.

Ferdous, W., Manalo, A., Siddique, R., Mendis, P., Zhuge, Y., Wong, H.S., Lokuge, W., Aravinthan, T., Schubel, P., 2021. Recycling of landfill wastes (tyres, plastics and glass) in construction–A review on global waste generation, performance, application and future opportunities. Resour. Conserv. Recycl. 173, 105745 https://doi.org/10.1016/j.resconrec.2021.105745.

Gao, Y., Yue, Q., Gao, B., Li, A., 2020. Insight into activated carbon from different kinds of chemical activating agents: a review. Sci. Total Environ. 746, 141094 https://doi.org/10.1016/j.scitotenv.2020.141094.

Gharagheizi, F., Sholl, D.S., 2021. Comprehensive assessment of the accuracy of the ideal adsorbed solution theory for predicting binary adsorption of gas mixtures in porous materials. Ind. Eng. Chem. Res. 61 (1), 727–739. https://doi.org/10.1021/acs.iecr.1c03876.

Global tire recycling market analysis 2025: opportunity, demand, growth and forecast 2017–2025—edition. Available online: https://www.goldsteinresearch.com/report/global-tire-recycling-industry-market-trends-analysis.

Gomez-Serrano, V., Valenzuela-Calahorro, C., Pastor-Villegas, J., 1993. Characterization of rockrose wood, char and activated carbon. Biomass Bioenergy 4 (5), 355–364. https://doi.org/10.1016/0961-9534(93)90052-6.

Gonzalez, J.F., Roman, S., González-García, C.M., Nabais, J.V., Ortiz, A.L., 2009. Porosity development in activated carbons prepared from walnut shells by carbon dioxide or steam activation. Ind. Eng. Chem. Res. 48 (16), 7474–7481. https://doi.org/10.1021/ie801848x.

Grundy, M., Ye, Z., 2014. Cross-linked polymers of diethynylbenzene and phenylacetylene as new polymer precursors for high-yield synthesis of high-performance nanoporous activated carbons for supercapacitors, hydrogen storage, and CO_2 capture. J. Mater. Chem. A 2 (47), 20316–20330. https://doi.org/10.1039/C4TA04038D.

Guclu, Y., Erer, H., Demiral, H., Altintas, C., Keskin, S., Tumanov, N., Su, B.L., Semerci, F., 2021. Oxalamide-functionalized metal organic frameworks for CO_2 adsorption. ACS Appl. Mater. Interfaces 13 (28), 33188–33198. https://doi.org/10.1021/acsami.1c11330.

Guo, Y., Tan, C., Sun, J., Li, W., Zhang, J., Zhao, C., 2020. Porous activated carbons derived from waste sugarcane bagasse for CO_2 adsorption. Chem. Eng. J. 381, 122736 https://doi.org/10.1016/j.cej.2019.122736.

Han, P., Yue, Y., Zhang, L., Xu, H., Liu, Z., Zhang, K., Zhang, C., Dong, S., Ma, W., Cui, G., 2012. Nitrogen-doping of chemically reduced mesocarbon microbead oxide for the improved performance of lithium ion batteries. Carbon 50 (3), 1355–1362. https://doi.org/10.1016/j.carbon.2011.11.007.

Hendricks, S.B., 1941. Base exchange of the clay mineral montmorillonite for organic cations and its dependence upon adsorption due to van der Waals forces. J. Phys. Chem. A 45 (1), 65–81. https://doi.org/10.1021/j150406a006.

Hoang, A.T., Varbanov, P.S., Nižetić, S., Sirohi, R., Pandey, A., Luque, R., Ng, K.H., Pham, V.V., 2022. Perspective review on Municipal Solid Waste-to-energy route: characteristics, management strategy, and role in circular economy. J. Clean. Prod., 131897 https://doi.org/10.1016/j.jclepro.2022.131897.

Hofman, M., Pietrzak, R., 2011. Adsorbents obtained from waste tires for NO_2 removal under dry conditions at room temperature. Chem. Eng. J. 170 (1), 202–208. https://doi.org/10.1016/j.cej.2011.03.054.

Idrees, M., Rangari, V., Jeelani, S., 2018. Sustainable packaging waste-derived activated carbon for carbon dioxide capture. J. CO2 Util. 26, 380–387. https://doi.org/10.1016/j.jcou.2018.05.016.

Irmer, G., Dorner-Reisel, A., 2005. Micro-Raman studies on DLC coatings. Adv. Eng. Mater. 7 (8), 694–705. https://doi.org/10.1002/adem.200500006.

Jagiello, J., Olivier, J.P., 2013. 2D-NLDFT adsorption models for carbon slit-shaped pores with surface energetical heterogeneity and geometrical corrugation. Carbon 55, 70–80. https://doi.org/10.1016/j.carbon.2012.12.011.

Jagiello, J., Kenvin, J., Celzard, A., Fierro, V., 2019a. Enhanced resolution of ultra micropore size determination of biochars and activated carbons by dual gas analysis using N_2 and CO_2 with 2D-NLDFT adsorption models. Carbon N. Y. 144, 206–215. https://doi.org/10.1016/j.carbon.2018.12.028.

Jagiello, J., Kenvin, J., Celzard, A., Fierro, V., 2019b. Enhanced resolution of ultra micropore size determination of biochars and activated carbons by dual gas analysis using N_2 and CO_2 with 2D-NLDFT adsorption models. Carbon 144, 206–215. https://doi.org/10.1016/j.carbon.2018.12.028.

Jjagwe, J., Olupot, P.W., Menya, E., Kalibbala, H.M., 2021. Synthesis and application of Granular activated carbon from biomass waste materials for water treatment: a review. Journal of Bioresources and Bioproducts 6 (4), 292–322. https://doi.org/10.1016/j.jobab.2021.03.003.

Kajal, A., Singh, R., 2019. Coriandrum sativum seeds extract mitigate progression of diabetic nephropathy in experimental rats via AGEs inhibition. PLoS One 14 (3), e0213147. https://doi.org/10.1371/journal.pone.0213147.

Kandasamy, J., Gökalp, I., 2015. Pyrolysis, combustion, and steam gasification of various types of scrap tires for energy recovery. Energy Fuel. 29 (1), 346–354. https://doi.org/10.1021/ef502283s.

Karaağaç, B., Ercan Kalkan, M., Deniz, V., 2017. End of life tyre management: Turkey case. J. Mater. Cycles Waste Manag. 19, 577–584. https://doi.org/10.1007/s10163-015-0427-2.

Khalil, S.H., Aroua, M.K., Daud, W.M.A.W., 2012. Study on the improvement of the capacity of amine-impregnated commercial activated carbon beds for CO_2 adsorbing. Chem. Eng. J. 183, 15–20. https://doi.org/10.1016/j.cej.2011.12.011.

Khoshraftar, Z., Ghaemi, A., 2023. Evaluation of CaO derived from Cerastoderma glaucum of Caspian beach as a natural sorbent for CO_2 capture. Current Research in Green and Sustainable Chemistry 6, 100360. https://doi.org/10.1016/j.crgsc.2023.100360.

Kishibayev, K.K., Serafin, J., Tokpayev, R.R., Khavaza, T.N., Atchabarova, A.A., Abduakhytova, D.A., Ibraimov, Z.T., Sreńscek-Nazzal, J., 2021. Physical and chemical properties of activated carbon synthesized from plant wastes and shungite for CO_2 capture. J. Environ. Chem. Eng. 9 (6), 106798 https://doi.org/10.1016/j.jece.2021.106798.

Lahuri, A.H., Khai, M.L.N., Rahim, A.A., Nordin, N., 2020. Adsorption kinetics for CO2 capture using cerium oxide impregnated on activated carbon. Acta Chim. Slov. 67, 570–580. https://doi.org/10.17344/acsi.2019.5572.

Lan, X., Jiang, X., Song, Y., Jing, X., Xing, X., 2019. The effect of activation temperature on structure and properties of blue coke-based activated carbon by CO_2 activation. Green Process. Synth. 8 (1), 837–845. https://doi.org/10.1515/gps-2019-0054.

Li, D., Ma, T., Zhang, R., Tian, Y., Qiao, Y., 2015. Preparation of porous carbons with high low-pressure CO_2 uptake by KOH activation of rice husk char. Fuel 139, 68–70. https://doi.org/10.1016/j.fuel.2014.08.027.

Li, S., Han, K., Li, J., Li, M., Lu, C., 2017. Preparation and characterization of super activated carbon produced from gulfweed by KOH activation. Microporous Mesoporous Mater. 243, 291–300. https://doi.org/10.1016/j.micromeso.2017.02.052.

Li, W., Li, X., Chang, W., Wu, J., Liu, P., Wang, J., Yao, X., Yu, Z.Z., 2020a. Vertically aligned reduced graphene oxide/Ti 3 C 2 T x MXene hybrid hydrogel for highly efficient solar steam generation. Nano Res. 13, 3048–3056. https://doi.org/10.1007/s12274-020-2970-y.

Li, F., Zhang, Y., Wang, S., Li, G., Yue, X., Zhong, D., Chen, C., Shen, K., 2020b. Insight into ex-situ thermal desorption of soils contaminated with petroleum via carbon number-based fraction approach. Chem. Eng. J. 385, 123946 https://doi.org/10.1016/j.cej.2019.123946.

López, F.A., Centeno, T.A., Rodríguez, O., Alguacil, F.J., 2013. Preparation and characterization of activated carbon from the char produced in the thermolysis of granulated scrap tyres. J. Air Waste Manag. Assoc. 63 (5), 534–544. https://doi.org/10.1080/10962247.2013.763870.

Martínez, J.D., 2021. An overview of the end-of-life tires status in some Latin American countries: proposing pyrolysis for a circular economy. Renew. Sustain. Energy Rev. 144, 111032 https://doi.org/10.1016/j.rser.2021.111032.

Merin, P., Jimmy Joy, P., Muraledharan, M.N., Veena Gopalan, E., Seema, A., 2021. Biomass-derived activated carbon for high-performance supercapacitor electrode applications. Chem. Eng. Technol. 44 (5), 844–851. https://doi.org/10.1002/ceat.202000450.

Mert, H., Deniz, C.U., Baykasoglu, C., 2023. Adsorptive separation of CH_4, H_2, CO_2, and N_2 using fullerene pillared graphene nanocomposites: insights from molecular simulations. J. Mol. Model. 29 (10), 315. https://doi.org/10.1007/s00894-023-05715-0.

Mistar, E.M., Alfatah, T., Supardan, M.D., 2020. Synthesis and characterization of activated carbon from Bambusa vulgaris striata using two-step KOH activation. J. Mater. Res. Technol. 9 (3), 6278–6286. https://doi.org/10.1016/j.jmrt.2020.03.041.

Mohajerani, A., Burnett, L., Smith, J.V., Markovski, S., Rodwell, G., Rahman, M.T., Kurmus, H., Mirzababaei, M., Arulrajah, A., Horpibulsuk, S., Maghool, F., 2020. Recycling waste rubber tyres in construction materials and associated environmental considerations: a review. Resour. Conserv. Recycl. 155, 104679 https://doi.org/10.1016/j.resconrec.2020.104679.

Mohan, A.N., Manoj, B., 2012. Synthesis and characterization of carbon nanospheres from hydrocarbon soot. Int. J. Electrochem. Sci. 7 (10), 9537–9549.

Mukherjee, S., Samanta, A.N., 2019. Amine-impregnated MCM-41 in post-combustion CO_2 capture: synthesis, characterization, isotherm modelling. Adv. Powder Technol. 30 (12), 3231–3240. https://doi.org/10.1016/j.apt.2019.09.032.

Mukherjee, A., Okolie, J.A., Abdelrasoul, A., Niu, C., Dalai, A.K., 2019. Review of post-combustion carbon dioxide capture technologies using activated carbon. J. Environ. Sci. 83, 46–63. https://doi.org/10.1016/j.jes.2019.03.014.

Muttakin, M., Mitra, S., Thu, K., Ito, K., Saha, B.B., 2018. Theoretical framework to evaluate minimum desorption temperature for IUPAC classified adsorption isotherms. Int. J. Heat Mass Tran. 122, 795–805. https://doi.org/10.1016/j.ijheatmasstransfer.2018.01.107.

Nandi, M., Uyama, H., 2014. Exceptional CO_2 adsorbing materials under different conditions. Chem. Rec. 14 (6), 1134–1148. https://doi.org/10.1002/tcr.201402062.

Nazir, G., Rehman, A., Park, S.J., 2021. Role of heteroatoms (nitrogen and sulfur)-dual doped corn-starch based porous carbons for selective CO_2 adsorption and separation. J. CO2 Util. 51, 101641 https://doi.org/10.1016/j.jcou.2021.101641.

Nieto-Márquez, A., Atanes, E., Morena, J., Fernández-Martínez, F., Valverde, J.L., 2016. Upgrading waste tires by chemical activation for the capture of SO_2. Fuel Process. Technol. 144, 274–281. https://doi.org/10.1016/j.fuproc.2016.01.009.

Nuhnen, A., Janiak, C., 2020. A practical guide to calculate the isosteric heat/enthalpy of adsorption via adsorption isotherms in metal–organic frameworks, MOFs. Dalton Trans. 49 (30), 10295–10307. https://doi.org/10.1039/D0DT01784A.

Ogungbenro, A.E., Quang, D.V., Al-Ali, K.A., Vega, L.F., Abu-Zahra, M.R., 2018. Physical synthesis and characterization of activated carbon from date seeds for CO_2 capture. J. Environ. Chem. Eng. 6 (4), 4245–4252.

Ogungbenro, A.E., Quang, D.V., Al-Ali, K.A., Vega, L.F., Abu-Zahra, M.R., 2020. Synthesis and characterization of activated carbon from biomass date seeds for carbon dioxide adsorption. J. Environ. Chem. Eng. 8 (5), 104257 https://doi.org/10.1016/j.jece.2020.104257.

Ould-Idriss, A., Stitou, M., Cuerda-Correa, E.M., Fernandez-Gonzalez, C., Marcias-Garcia, A., Alexandre-Franco, M.F., Gomez-Serrano, V., 2011. Preparation of activated carbons from olive-tree wood revisited. II. Physical activation with air. Fuel Process. Technol. 92, 266–270. https://doi.org/10.1016/j.fuproc.2010.05.018.

Ozpinar, P., Dogan, C., Demiral, H., Morali, U., Erol, S., Samdan, C., Yildiz, D., Demiral, I., 2022. Activated carbons prepared from hazelnut shell waste by phosphoric acid activation for supercapacitor electrode applications and comprehensive electrochemical analysis. Renew. Energy 189, 535–548. https://doi.org/10.1016/j.renene.2022.02.126.

Parshetti, G.K., Chowdhury, S., Balasubramanian, R., 2015. Biomass derived low-cost microporous adsorbents for efficient CO_2 capture. Fuel 148, 246–254. https://doi.org/10.1016/j.fuel.2015.01.032.

Plaza, M.G., Pevida, C., Martín, C.F., Fermoso, J., Pis, J.J., Rubiera, F., 2010. Developing almond shell-derived activated carbons as CO_2 adsorbents. Separ. Purif. Technol. 71 (1), 102–106. https://doi.org/10.1016/j.seppur.2009.11.008.

Plaza, M.G., González, A.S., Pis, J.J., Rubiera, F., Pevida, C., 2014. Production of microporous biochars by single-step oxidation: effect of activation conditions on CO_2 capture. Appl. Energy 114, 551–562. https://doi.org/10.1016/j.apenergy.2013.09.058.

Premchand, P., Demichelis, F., Chiaramonti, D., Bensaid, S., Fino, D., 2023. Biochar production from slow pyrolysis of biomass under CO_2 atmosphere: a review on the effect of CO_2 medium on biochar production, characterisation, and environmental applications. J. Environ. Chem. Eng. 110009 https://doi.org/10.1016/j.jece.2023.110009.

Raganati, F., Ammendola, P., Chirone, R., 2014. CO_2 adsorption on fine activated carbon in a sound assisted fluidized bed: effect of sound intensity and frequency, CO_2 partial pressure and fluidization velocity. Appl. Energy 113, 1269–1282. https://doi.org/10.1016/j.apenergy.2013.08.073.

Sait, H.H., Hussain, A., Salema, A.A., Ani, F.N., 2012. Pyrolysis and combustion kinetics of date palm biomass using thermogravimetric analysis. Bioresour. Technol. 118, 382–389. https://doi.org/10.1016/j.biortech.2012.04.081.

Sangchoom, W., Mokaya, R., 2015. Valorization of lignin waste: carbons from hydrothermal carbonization of renewable lignin as superior sorbents for CO_2 and hydrogen storage. ACS Sustain. Chem. Eng. 3 (7), 1658–1667. https://doi.org/10.1021/acssuschemeng.5b00351.

Serafin, J., Dziejarski, B., 2023. Application of isotherms models and error functions in activated carbon CO_2 sorption processes. Microporous Mesoporous Mater. 354, 112513 https://doi.org/10.1016/j.micromeso.2023.112513.

Serafin, J., Narkiewicz, U., Morawski, A.W., Wróbel, R.J., Michalkiewicz, B., 2017. Highly microporous activated carbons from biomass for CO_2 capture and effective micropores at different conditions. J. CO2 Util. 18, 73–79. https://doi.org/10.1016/j.jcou.2017.01.006.

Serafin, J., Baca, M., Biegun, M., Mijowska, E., Kaleńczuk, R.J., Sreńscek-Nazzal, J., Michalkiewicz, B., 2019. Direct conversion of biomass to nanoporous activated biocarbons for high CO_2 adsorption and supercapacitor applications. Appl. Surf. Sci. 497, 143722 https://doi.org/10.1016/j.apsusc.2019.143722.

Serafin, J., Ouzzine, M., Junior, O.F.C., Sreńscek-Nazzal, J., 2021. Preparation of low-cost activated carbons from amazonian nutshells for CO_2 storage. Biomass Bioenergy 144, 105925. https://doi.org/10.1016/j.biombioe.2020.105925.

Serafin, J., Kiełbasa, K., Michalkiewicz, B., 2022a. The new tailored nanoporous carbons from the common polypody (Polypodium vulgare): the role of textural properties for enhanced CO_2 adsorption. Chem. Eng. J. 429, 131751 https://doi.org/10.1016/j.cej.2021.131751.

Serafin, J., Sreńscek-Nazzal, J., Kamińska, A., Paszkiewicz, O., Michalkiewicz, B., 2022b. Management of surgical mask waste to activated carbons for CO_2 capture. J. CO2 Util. 59, 101970 https://doi.org/10.1016/j.jcou.2022.101970.

Serafin, J., Dziejarski, B., Sreńscek-Nazzal, J., 2023a. An innovative and environmentally friendly bioorganic synthesis of activated carbon based on olive stones and its potential application for CO_2 capture. Sustainable Materials and Technologies 38, e00717. https://doi.org/10.1016/j.susmat.2023.e00717.

Serafin, J., Dziejarski, B., Junior, O.F.C., Sreńscek-Nazzal, J., 2023b. Design of highly microporous activated carbons based on walnut shell biomass for H_2 and CO_2 storage. Carbon 201, 633–647. https://doi.org/10.1016/j.carbon.2022.09.013.

Shahkarami, S., Azargohar, R., Dalai, A.K., Soltan, J., 2015. Breakthrough CO_2 adsorption in bio-based activated carbons. J. Environ. Sci. 34, 68–76. https://doi.org/10.1016/j.jes.2015.03.008.

Shen, F., Wang, Y., Li, L., Zhang, K., Smith, R.L., Qi, X., 2018. Porous carbonaceous materials from hydrothermal carbonization and KOH activation of corn stover for highly efficient CO_2 capture. Chem. Eng. Commun. 205 (4), 423–431. https://doi.org/10.1080/00986445.2017.1367671.

Singh, R.K., Ruj, B., Jana, A., Mondal, S., Jana, B., Sadhukhan, A.K., Gupta, P., 2018. Pyrolysis of three different categories of automotive tyre wastes: product yield analysis and characterization. J. Anal. Appl. Pyrol. 135, 379–389. https://doi.org/10.1016/j.jaap.2018.08.011.

Soltani, R., Marjani, A., Shirazian, S., 2019. Facile one-pot synthesis of thiol-functionalized mesoporous silica submicrospheres for Tl (I) adsorption: isotherm, kinetic and thermodynamic studies. J. Hazard Mater. 371, 146–155. https://doi.org/10.1016/j.jhazmat.2019.02.076.

Sricharoenchaikul, V., Pechyen, C., Aht-ong, D., Atong, D., 2008. Preparation and characterization of activated carbon from the pyrolysis of physic nut (Jatropha curcas L.) waste. Energy Fuel. 22 (1), 31–37. https://doi.org/10.1021/ef700285u.

Stavropoulos, G.G., 2005. Precursor materials suitability for super activated carbons production. Fuel Process. Technol. 86 (11), 1165–1173. https://doi.org/10.1016/j.fuproc.2004.11.011.

Sun, J., Brady, T.A., Rood, M.J., Lehmann, C.M., Rostam-Abadi, M., Lizzio, A.A., 1997. Adsorbed natural gas storage with activated carbons made from Illinois coals and scrap tires. Energy Fuel. 11 (2), 316–322. https://doi.org/10.1021/ef960201h.

Sun, D.L., Wang, F., Hong, R.Y., Xie, C.R., 2016. Preparation of carbon black via arc discharge plasma enhanced by thermal pyrolysis. Diam. Relat. Mater. 61, 21–31. https://doi.org/10.1016/j.diamond.2015.11.004.

Talik, P., Moskal, P., Proniewicz, L.M., Wesełucha-Birczyńska, A., 2020. The Raman spectroscopy approach to the study of Water–Polymer interactions in hydrated hydroxypropyl cellulose (HPC). J. Mol. Struct. 1210, 128062 https://doi.org/10.1016/j.molstruc.2020.128062.

Tang, Z., Gao, J., Zhang, Y., Du, Q., Feng, D., Dong, H., Peng, Y., Zhang, T., Xie, M., 2023. Ultra-microporous biochar-based carbon adsorbents by a facile chemical activation strategy for high-performance CO_2 adsorption. Fuel Process. Technol. 241, 107613 https://doi.org/10.1016/j.fuproc.2022.107613.

Teng, H., Lin, Y.C., Hsu, L.Y., 2000. Production of activated carbons from pyrolysis of waste tires impregnated with potassium hydroxide. J. Air Waste Manag. Assoc. 50 (11), 1940–1946. https://doi.org/10.1080/10473289.2000.10464221.

Thonglhueng, N., Sirisangsawang, R., Sukpancharoen, S., Phetyim, N., 2022. Optimization of iodine number of carbon black obtained from waste tire pyrolysis plant via response surface methodology. Heliyon 8 (12). https://doi.org/10.1016/j.heliyon.2022.e11971.

Thote, J.A., Iyer, K.S., Chatti, R., Labhsetwar, N.K., Biniwale, R.B., Rayalu, S.S., 2010. In situ nitrogen enriched carbon for carbon dioxide capture. Carbon 48 (2), 396–402. https://doi.org/10.1016/j.carbon.2009.09.042.

Tian, X., Zhuang, Q., Han, S., Li, S., Liu, H., Li, L., Zhang, J., Wang, C., Bian, H., 2021. A novel approach of reapplication of carbon black recovered from waste tyre pyrolysis to rubber composites. J. Clean. Prod. 280, 124460 https://doi.org/10.1016/j.jclepro.2020.124460.

Trudsø, L.L., Nielsen, M.B., Hansen, S.F., Syberg, K., Kampmann, K., Khan, F.R., Palmqvist, A., 2022. The need for environmental regulation of tires: challenges and recommendations. Environ. Pollut. 311, 119974 https://doi.org/10.1016/j.envpol.2022.119974.

Wang, Y., Alsmeyer, D.C., McCreery, R.L., 1990. Raman spectroscopy of carbon materials: structural basis of observed spectra. Chem. Mater. 2 (5), 557–563. https://doi.org/10.1021/cm00011a018.

Wang, S., Nam, H., Nam, H., 2020. Preparation of activated carbon from peanut shell with KOH activation and its application for H_2S adsorption in confined space. J. Environ. Chem. Eng. 8 (2), 103683 https://doi.org/10.1016/j.jece.2020.103683.

Wei, P.S., Hsieh, Y.C., Chiu, H.H., Yen, D.L., Lee, C., Tsai, Y.C., Ting, T.C., 2018. Absorption coefficient of carbon dioxide across atmospheric troposphere layer. Heliyon 4 (10). https://doi.org/10.1016/j.heliyon.2018.e00785.

Xuguang, S., 2005. The investigation of chemical structure of coal macerals via transmitted-light FT-IR microspectroscopy. Spectrochim. Acta Mol. Biomol. Spectrosc. 62 (1–3), 557–564. https://doi.org/10.1016/j.saa.2005.01.020.

Yang, F., Liang, S., Wu, H., Yue, C., Yan, H., Wu, H., Chen, X., Zhang, J., Yan, S., Duan, Y., 2022. Upgrading the pyrolysis carbon black from waste tire by hybridization with cellulose. Ind. Eng. Chem. Res. 61 (19), 6512–6520. https://doi.org/10.1021/acs.iecr.2c00601.

Yousif, Q.A., Ranjeh, M., Ghiyasiyan-Arani, M., Al-Nayili, A., Monsef, R., Salavati-Niasari, M., 2022. Morphology engineering of $LiFeO_2$ nanostructures through synthesis controlling for electrochemical hydrogen storage inquiries. Fuel 313, 123025. https://doi.org/10.1016/j.fuel.2021.123025.

Yue, M.B., Sun, L.B., Cao, Y., Wang, Z.J., Wang, Y., Yu, Q., Zhu, J.H., 2008. Promoting the CO_2 adsorption in the amine-containing SBA-15 by hydroxyl group. Microporous Mesoporous Mater. 114 (1–3), 74–81. https://doi.org/10.1016/j.micromeso.2007.12.016.

Zabaniotou, A., Stavropoulos, G., Skoulou, V., 2008. Activated carbon from olive kernels in a two-stage process: industrial improvement. Bioresour. Technol. 99 (2), 320–326. https://doi.org/10.1016/j.biortech.2006.12.020.

Zhang, Y., Tao, L., Xie, C., Wang, D., Zou, Y., Chen, R., Wang, Y., Jia, C., Wang, S., 2020. Defect engineering on electrode materials for rechargeable batteries. Adv. Mater. 32 (7), 1905923 https://doi.org/10.1002/adma.201905923.